

Video-based monitoring of the Egmond beach- and shoreface nourishments

M. Caljouw

September, 2000

Preface

This report, which serves as my M.Sc. thesis, describes a study within the framework of the studies Civil Engineering at the Faculty of Civil Engineering and Geosciences, Hydraulic and Offshore Engineering Division of Delft University of Technology.

The study concerns the behaviour and effects of the beach- and shoreface nourishments at Egmond. This has been done with the help of several Argus image processing techniques.

The study has been carried out at WL| Delft Hydraulics. The work was performed in assignment for Rijkswaterstaat RIKZ, under the project number Z2773.

This project was (partly) funded by the Delft Cluster Project Coasts 03.01.03.

I would like to thank my supervisors, prof.dr.ir.M.J.F.Stive (Delft University of Technology and WL | Delft Hydraulics), ir. S.G.J. Aarninkhof (Delft University of Technology and WL | Delft Hydraulics) , drs.S.E. Hoogewoning (RIKZ, Rijkswaterstaat), Prof. Dr. ing. R.A.P. Klees (Delft University of Technology) for sharing their knowledge and support during this study. Furthermore, I would like to thank my temporary colleagues and fellow graduate students at WL | Delft Hydraulics for showing their interest and making my stay very pleasant. And last but not least, I want to thank my family and girlfriend for their support during the years I spent in Delft.

Contents

Preface1

Summary (in Dutch)..... 1

1 Introduction 1-1

1.1 In general 1-1

1.2 Problem definition..... 1-1

1.3 Objectives of this study 1-3

1.4 Approach 1-3

1.5 Reading guide..... 1-3

2 The Argus video system 2-1

2.1 Introduction 2-1

2.2 The ARGUS program 2-1

2.3 Image processing 2-2

2.3.1 Introduction 2-2

2.3.2 The rectification process 2-2

2.3.3 Pixel resolution..... 2-5

2.4 Egmond site ‘Jan van Speijk’ 2-6

2.5 Standard post-processing tools..... 2-7

3 Waterline detection model..... 3-1

3.1 Introduction 3-1

3.2 Determination of the X,Y-coordinates 3-2

3.2.1 Pixel clustering based on color information..... 3-2

3.2.2 Testing the discrimination of pixels: 3-5

3.2.3 Interpolation to waterline coordinates..... 3-6

3.2.4 Evaluation waterline detection technique 3-7

3.3 Modelling the Z-coordinate 3-9

3.3.1 The measured waterlevel offshore 3-9

3.3.2 The wave setup using UNIBEST-TC 3-10

3.3.3	Wind setup.....	3-11
3.3.4	Swash (run-up and run-down)	3-12
3.3.5	Surfbeat	3-13
3.3.6	The individual contribution of each component	3-13
4	Model validation with field measurements	4-1
4.1	Introduction	4-1
4.2	Approach to field measurements	4-1
4.3	Field measurements	4-2
4.3.1	DGPS-measurements.....	4-2
4.3.2	Swash-measurements	4-4
4.3.3	Additional observations	4-5
4.4	Results and conclusions of the measurements	4-6
4.4.1	Waterline measurements.....	4-6
4.4.2	Video recordings of the swash zone	4-8
4.4.3	Summarising the results	4-9
4.5	Model validation	4-9
4.5.1	Validation waterline detection technique	4-10
4.5.2	Validation of the waterline height	4-12
4.5.3	Validation of the whole model	4-13
5	Evaluation of the Egmond beach- and shoreface nourishments between June 1999 and June 2000	5-1
5.1	Introduction	5-1
5.2	Sand nourishments	5-1
5.2.1	Nourishing in general	5-1
5.2.2	Beach nourishments in general	5-2
5.2.3	Beach nourishment in combination with a shoreface nourishment at Egmond.....	5-3
5.3	Intertidal beach morphology	5-4
5.4	Bar behaviour	5-7
5.5	Beach width.....	5-9
6	Conclusions and recommendations	6-1
6.1	Introduction	6-1
6.2	Conclusions	6-1
6.2.1	Model	6-1
6.2.2	Application.....	6-2

6.3	Recommendations	6-3
6.3.1	Model	6-3
6.3.2	Application	6-4
References		Lit.-1

Appendices

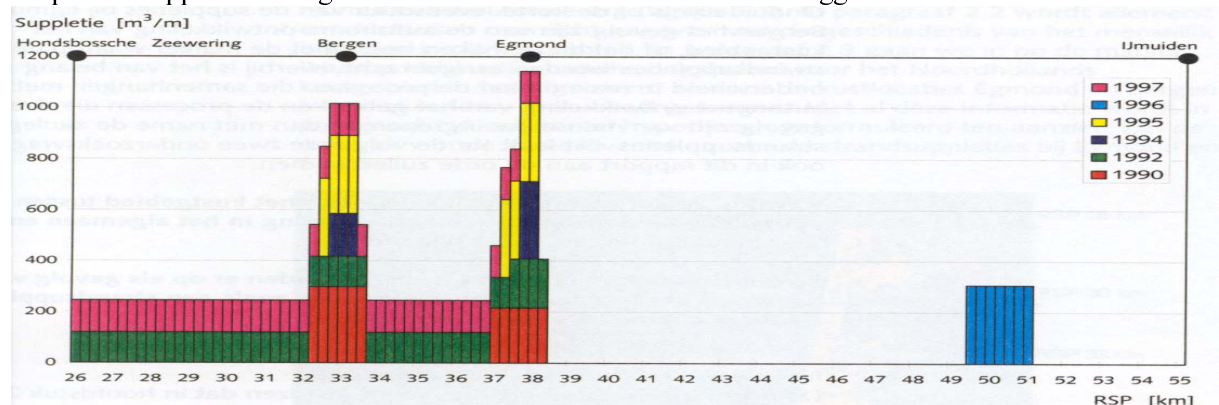
- A Existing Argus based methods for finding the waterline**
- B Cases at where the waterline detection model is not appreciable**
- C Calculations for the vertical waterline coordinate**
- D Results from the swash videos**
- E Waterline measurements**
- F Egmond morphology**

Summary (in Dutch)

Inleiding

Delen van de Nederlandse kust verliezen structureel zand (erosie), door de werking van getij en golven. Hierdoor trekt de kust zich lokaal landwaarts terug. Om de kustachteruitgang tegen te gaan is in 1990 de Basiskustlijn (BKL) gedefinieerd en is besloten om de ligging van de kustlijn per 1 januari 1990 te handhaven. Wanneer deze norm in gevaar komt, wordt het verlies van zand weer aangevuld middels zandsuppleties.

Rond de badplaatsen Egmond aan Zee en Bergen, aan de Noordhollandse kust, zijn veel frequenter suppleties nodig om de BKL te handhaven dan in de omliggende kustvakken.



Figuur 1 Suppletiehoeveelheden langs de Hollandse kust

De grotere suppletiefrequentie brengt hogere onderhoudskosten met zich mee en bij de uitvoering van zandsuppleties op het strand wordt de recreatie verstoord.

Twee oorzaken voor de korte levensduur van de suppleties zijn denkbaar. Ten eerste is het mogelijk dat de aanwezigheid van zogenaamde muisystemen een snellere zeewaartse afvoer van zand veroorzaakt. Ten tweede ligt de BKL ter plaatse verder zeewaarts dan in de omliggende kustvakken; dit om het risico van overstroming van de boulevard te beperken. Een snellere verspreiding van het gesuppleerde zand naar aanliggende kustvakken kan hiervan het gevolg zijn.

Als alternatieve oplossingsrichting is in het KUST*2000 programma een combinatie van strand- en vooroeversuppletie voorgesteld. De strandsuppletie handhaaft in eerste instantie de BKL. De verwachting is dat bij aanwezigheid van de vooroeversuppletie een soort luwtegebied ontstaat aan de landwaartse zijde. Het langstransport van zand zal hierdoor afnemen en de strandsuppletie wordt tegen golfaanval beschermt. Door kustdwars zandtransport kan de vooroeversuppletie het strand wellicht “voeden”. Een langere levensduur van de suppletie is het verwachte resultaat.

In 1999 is de combinatie van strand- en vooroeversuppletie uitgevoerd bij Egmond aan Zee. Om de ontwikkeling van beide suppleties te monitoren is onder meer in mei 1999 een Argus video station geïnstalleerd op de top van de vuurtoren “Jan van Speijk”. Dit Argus station bestaat uit 5 camera’s die ieder gericht zijn op een deel van de kust. Elk uur legt elke camera drie soorten beelden vast die worden opgeslagen in een database. In deze studie worden tijdsgemiddelde beelden gebruikt, de individuele golven zijn in zulke beelden uitgefilterd en alleen de gemiddelde golfcondities zijn zichtbaar.

Het doel van deze studie is een evaluatie te geven van het effect en gedrag van beide supplementen, hierbij gebruik makende van verschillende Argus video technieken toegepast op de tijdsgemiddelde beelden van het Argus video station in Egmond aan Zee.

Validatie van het Argus waterlijn detectie model

De meest belangrijke Argus techniek voor deze studie is een waterlijn detectie model. Hiermee kan de positie van de waterlijn in 3D ruimte worden bepaald. Door meerdere waterlijnen te verzamelen binnen een getijcyclus kan hiermee de ligging het intergetijdestrand worden bepaald.

Het waterlijn detectie model bestaat uit twee delen:

De horizontale ligging van de waterlijn wordt bepaald uit Argus beelden. Op basis van kleurverschillen tussen droog en nat strand worden droge en natte pixels gescheiden. De scheidingslijn hiertussen representeert de waterlijn in het horizontale vlak.

De hoogte van de waterlijn wordt geschat door hydrodynamisch modelleren. Uitgangspunt hiervan is het gemeten getij op zee. De hoogte van de waterlijn wordt vervolgens gevonden door de bijdragen van golf opzet en golfloop (surfbeat en swash) hierbij op te tellen. De golf opzet wordt geschat met het model Unibest TC, de golfloop met empirische formules.

Om de nauwkeurigheid van het waterlijn detectie model te bepalen zijn waterlijn veldmetingen gedaan. Gedurende vier dagen, verdeeld over twee meetcampagnes, zijn met een jeep DGPS metingen van de waterlijn uitgevoerd. De metingen zijn gebruikt voor een onafhankelijke validatie van enerzijds de methode voor bepalen van de horizontale ligging van de waterlijn en anderzijds de methode voor de hoogte van de waterlijn.

De root mean square fout voor de ligging van de waterlijn in horizontale zin bleek ongeveer 6 m te zijn (6 tot 16 waterlijnen). De root mean square fout voor de verticale ligging is ongeveer 10 cm (27 waterlijnen). Voor het gehele model, uitgedrukt in een fout in verticale richting bleek dit ongeveer 15 cm (6 tot 16 waterlijnen).

Analyse van Argus videobeelden

Vervolgens is de waterlijn detectie techniek gebruikt voor het maken van intergetijdeprofielen in Egmond. Voor elke maand tussen Juni 1999 en Juni 2000 zijn op dagen met goede kwaliteit Argus beelden waterlijnen verzameld binnen het intergetijdestrand (tussen NAP 0 en NAP +1 m). Het resultaat is een serie van intergetijdestranden in de tijd, waaruit veranderingen in de strandligging kunnen worden afgeleid.

Om het inzicht in het morfologisch gedrag van het systeem te vergroten (met name het gedrag van zandbanken) is ook gebruik gemaakt van zogenaamde compositiebeelden. Door tijdsgemiddelde Argus beelden aan elkaar te plakken en te projecteren op het grondvlak ontstaat een bovenaanzicht van de kustzone van Egmond.

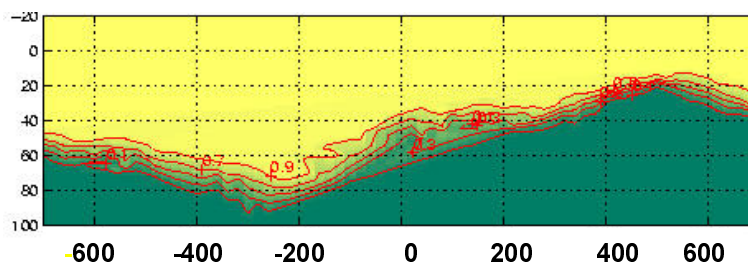


Figuur 2 Compositiebeelden

De witte banden die hierop zichtbaar zijn representeren de locaties waar golven breken (ondieptes) en corresponderen met de positie van zandbanken. Ook de vooroeversuppletie is als “zandbank” zichtbaar. Op basis van een serie van compositiebeelden tussen juni 1999 t/m juni 2000 kan de verschuiving van zandbankposities worden bepaald.

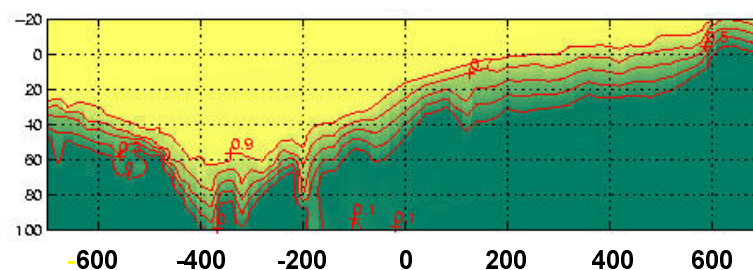
Observaties

Uit de reeks bepaalde intergetijdestranden (juni 1999 - juni 2000) valt op te maken dat de breedte van het strand niet gelijk is langs de kust. Aan de zuidzijde van het suppletiegebied is het strand smaller dan aan de noordzijde, met het zwaartepunt (breedste strand) juist ten noorden van het centrum van het suppletiegebied.



Figuur 3 Intergetijdestrand Juni 1999

In de wintermaanden oktober 1999 t/m februari 2000 vindt een versmalling van het (droge) strand plaats over het gehele suppletiegebied, terwijl er in de maanden maart 2000 t/m juni 2000 weer een verbreding (herstel) van het strand optreedt. Laatstgenoemd herstel vindt echter overwegend plaats aan de noordelijke helft van het suppletiegebied. Hierdoor is een groter verschil in (droge) strandbreedte ontstaan tussen het noordelijk en zuidelijk deel van de suppletiezone.



Figuur 4 Intergetijdestrand Juni 2000

Uit de compositiebeelden tussen juni 1999 en juni 2000 valt in eerste instantie op te maken dat de vooroeversuppletie als “zandbank” zichtbaar is en dat deze in de tijd landwaarts verschuift. Daarnaast is af te leiden dat de voormalig buitenste zandbank niet uniform in hoogte is; aan de noordzijde is meer energiedissipatie dan aan de zuidzijde. Vermoedelijk is de voormalige buitenste zandbank aan de noordzijde hoger. Verder verschuift de voormalige buitenste zandbank in de loop van de tijd landwaarts, terwijl de autonome verplaatsing van de zandbanken zeewaarts is (Wijnberg, 1995).

Rond het centrum van het suppletiegebied verschuiven de twee meest landwaartse (“binnenste”) zandbanken gedeeltelijk zeewaarts en liggen gebogen rondom de uitbouw van het strand nabij het centrum van het suppletiegebied.

Tot slot kan worden waargenomen dat onderbrekingen in de tweede binnenste zandbank, zogenaamde muilen, aanwezig zijn in de maanden juni t/m augustus 1999.

Hypotheses ontwikkeling strand- en vooroeversuppletie

Gebaseerd op bovengenoemde observaties met het Argus videosysteem zijn de volgende twee hypothesen opgesteld:

- I De aanwezigheid van de vooroeversuppletie verstoort het bankensysteem lokaal (uit evenwicht), waardoor als reactie hierop het bankensysteem zich wil aanpassen naar het oorspronkelijke drie- bankensysteem
- II De voormalig buitenste zandbank stuurt de ontwikkeling van het intergetijdestrand, de niet-uniformiteit in de bankhoogte resulteert in een niet-uniforme strandontwikkeling

Aanbevelingen

Nabewerking huidige resultaten

- bepaal de droge strandbreedte volgens RWS-definities en vergelijk deze met de langjarige ontwikkeling; onderscheid de invloed van seizoensfluctuaties in de strandbreedte van de niet-uniforme bijdrage

Monitoring/argus analysetechnieken

- continueer huidige aanpak van monitoring met Argus-beelden (hypothesevorming)
- gebruik lokale waterstandsmetingen tezamen met empirische formules voor nauwkeuriger berekening van de verticale positie van de waterlijn

Vervolgonderzoek

- bestudeer lodingen voor profielinformatie en bankpositie/hoogte; zandbalans voor check of landwaartse verschuiving vooroeversuppletie en voormalige buitenste brekerbank samenvalt met netto landwaarts zandtransport - voedingsmechanisme
- gebruik ook numerieke modellen

I Introduction

I.1 In general

The protection of the Dutch hinterland from flooding is mainly guaranteed by a sandy coast. It is this area of bars, beaches and dunes which is constantly under the influence of the elements of wind and water causing it to be a highly dynamic region. The ongoing occurrence of erosion events and periods of accretion justifies periodic monitoring of the coast.

The traditional way of monitoring has been done on a yearly basis. Since 1963 the position of the coastline is determined by measuring so called 'JARKUS' transects. This means that once a year the cross-shore profile is determined every 250 m longshore. This information is then stored in a database. Time series of 'jarkus' data indicate changes in profiles and the development of the position of the coastline.

Still, there are limitations with respect to the time scale. Morphologic changes on a shorter time scale such as seasonal fluctuations or the impact of a single event can not be determined. More insight in the behaviour of the coast on a shorter timescale might help to better understand the morphologic processes. Such information could contribute importantly to a more effective and cost diminishing approach towards coastal protection.

One way of coastal monitoring on a shorter time-scale is with the help of Argus video cameras. In 1992 the Argus program started, initiated by the Coastal Imaging Lab of the Oregon State University, USA by Prof. Holman. The technique is based on hourly made video images of (a part of) the coast by one or more fully automatic video cameras. Information from these images can be used to assess morphologic processes against low costs.

Nowadays over ten Argus stations are situated around the world. In the framework of this study the images of Argus station 'Jan van Speijk' at Egmond aan Zee, the Netherlands are used for coastal management purposes. The Argus image information is analysed to obtain useful knowledge about the local morphological changes and processes at Egmond.

I.2 Problem definition

The Dutch coast at Egmond is a sandy, inlet free, wave dominated coast where nourishments of sand are necessary to compensate erosion. In comparison with other parts of the Dutch coast the nourished sand disappears relatively fast: former maintenance nourishments with a design life span of five years lasted only for two years.

The main reason for this is a seaward shifted Basal Coast Line (BCL)* at Egmond. As the buildings on the boulevard are so close to the shore this buffer is necessary to reduce the risks of flooding (once every 500 years).

* In 1990 the Dutch government decided to combat structural erosion and made it her policy to maintain the location of the coastline. They introduced The Basal Coastline (BCL), corresponding to the location of the coastline at its position of the first of January 1990. In 1995 the local BCL has been redefined near Egmond aan Zee, which resulted in a seaward shifted BCL in front of the Egmond Boulevard.

Furthermore it concerns tourism and recreation, beach pavilion owners complain at local authorities when there is insufficient beach width.

In the past, the relative fast rate of net erosion, seasonal fluctuations in beach width and the importance of coastal protection lead to intervening nourishments to maintain the BCL. Due to the seaward shift of the BCL at Egmond a higher nourishment frequency is needed. As a result, a high nourishment frequency disturbs beach recreation and the large amounts of sand needed lead to high maintenance costs.

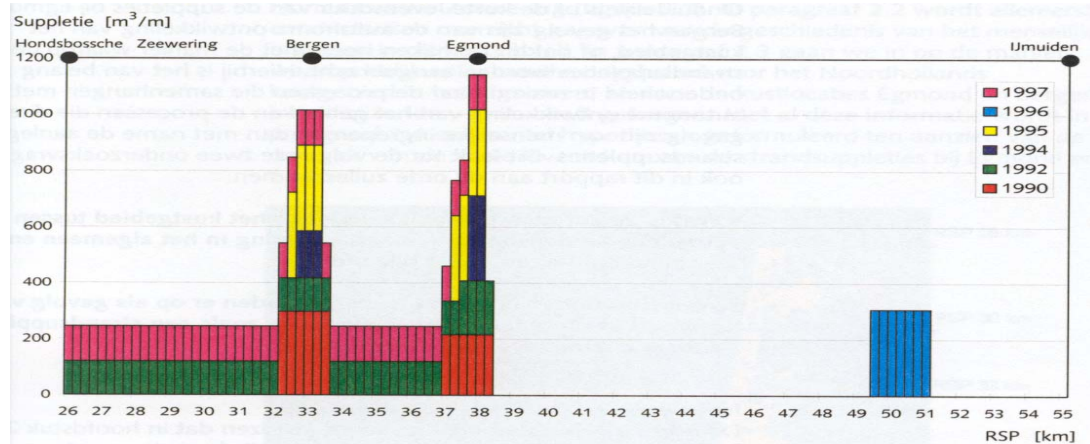


Figure 1.1 The amount of beach nourishments in the coastal area near Egmond between 1990 and 1997 (Boers, 2000)

Figure 1.1 shows the nourishment efforts between 1990 and 1997 for the coastal area between Hondsbosche Zeewering and IJmuiden. On the x-axis RSP means ‘Rijks Strand Paal’, indicating beach poles which have been placed every kilometer along the Dutch coast, starting north in Den Helder. This figure shows that during this period almost all nourishments have been carried out at the northern part of North Holland. The high nourishment frequencies in Bergen and Egmond are clearly visible.

The policy however is still to maintain a dynamic coast with long term nourishment programmes. It is therefore necessary to better understand the coastal processes at Egmond and to study the behaviour and efficiency of nourishment's.

The latest intervention to combat erosion took place in the spring of 1999. This concerns a beach nourishment of 200 m³/m over a length of 1.5 km, followed by a 400 m³/m shoreface nourishment over a length of 2200 m at depths bigger than 5 m. The centre of both nourishment's is located around kilometre transect 38.00. Special attention here goes to the shoreface nourishment, which is a relative new method of nourishing.

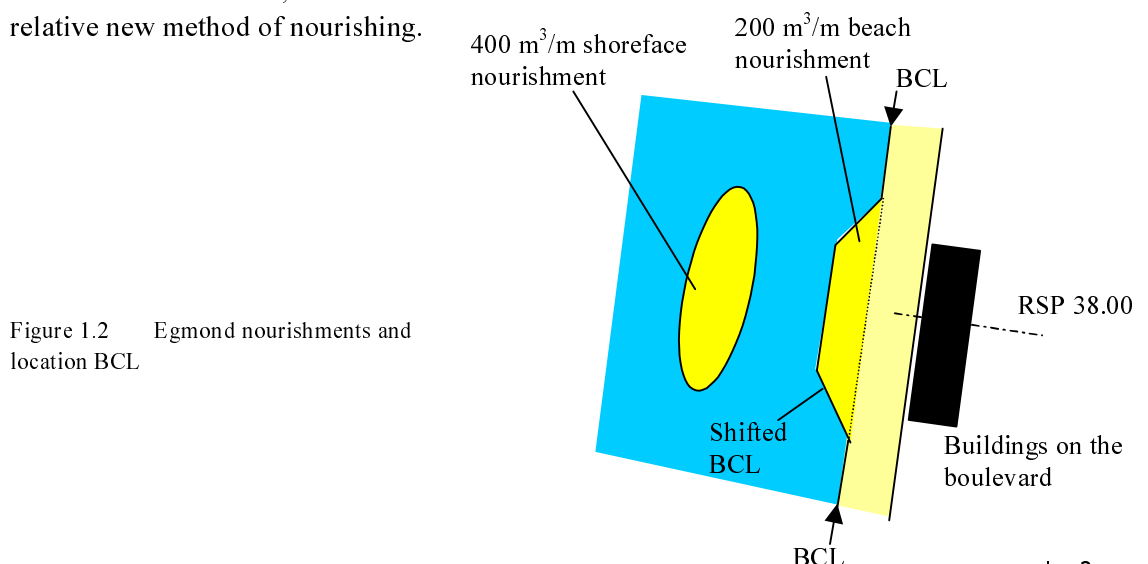


Figure 1.2 Egmond nourishments and location BCL

To monitor both of these nourishments, an Argus video system has been installed on the lighthouse ‘Jan van Speijk’ in may 1999. With hourly images, the development of the beach, the beach nourishment and the change in position of the shoreface nourishment can be followed.

1.3 Objectives of this study

The work in this study is focussed on the application of video monitoring in support of coastal management at Egmond, based on the first year of data from the ‘Jan van Speijk’ Argus station. By using several Argus techniques and tools the Argus image information can be rendered into useful results with respect to the Egmond coastal problemacy. These results should make it possible to evaluate the development of the combined beach and shoreface nourishment at Egmond, which is the main objective of this study.

The evaluation of both nourishments will be done in terms of :

1. Beach width

This is the area between the dune foot and the high waterline. Maintaining this part of the beach is especially important for recreation/tourism. Beside the beach nourishment it is expected that the shoreface nourishment will have a positive effect on the beach width.

2. Morphologic changes of the intertidal beach

The intertidal beach is the area between the low- and high waterline. Morphologically seen this is the most active part of the shore. Changes within the intertidal area will reflect the effect of both nourishment.

3. The behaviour of the shoreface nourishment itself

1.4 Approach

The most important Argus technique that will be used for the evaluation is the waterline detection model, which will be treated in chapter 3. Nevertheless the waterline detection model is a new technique that has been tested on a small scale and has not practically been used before. This means the model itself has to be evaluated first to get better insight in the applicability. Besides, it is necessary to compare model results with field measurements in order to find the accuracy of the model. Finally the modelling of waterlines can be used for modelling intertidal beach profiles.

The techniques of merged- and stacked images (see section 2.5) will also contribute to achieving the main objective. Time series of merged images should make clear how the shoreface nourishment behaves and moves. Stacked images on different transects will also support this.

Merged images also indicate the shoreline, and may be of use for finding the beach width and waterline.

1.5 Reading guide

The layout of this report is as follows:

First of all, chapter 2 starts with a description about the history and principals of the Argus video system. Going through this chapter it is explained how image information can be

processed into real world information. Furthermore the Argus station at Egmond aan Zee is treated in more detail. The last paragraph briefly describes some of the available Argus post-processing tools that have been applied on the Egmond images, including the waterline detection model.

Chapter 3 treats the waterline detection model itself. Here it is explained how to obtain horizontal waterline coordinates from time averaged Argus images. The vertical waterline coordinates are obtained by hydrodynamic modelling.

In chapter 4 the model for finding the waterline is validated with the help of field measurements. A comparison between waterline model results and waterline measurements indicates the accuracy of the model.

Besides, from observations in the field and the results of the measurements some conclusions can be drawn about the applicability of the model.

In chapter 5 the application of the waterline detection technique on the Egmond Argus images leads to determination of the intertidal beach morphology. Together with the techniques of ‘merged-’ and ‘stacked’ images useful information about the behaviour and effect of the beach- and shoreface nourishment can be obtained.

Finally chapter 6 describes the conclusions and recommendations that follow from this study.

2 The Argus video system

2.1 Introduction

The name ARGUS comes from the Argus who, in Greek mythology, was a giant with hundred eyes, ordered by Hera to watch Io. Nowadays it also refers to the video system developed at the Coastal Imaging Lab, Oregon State University (USA) under the guidance of professor R.A. Holman.

The history behind video imaging in nearshore studies goes probably back to the 1940s, where coastal processes were studied using some sort of image processing. The first attempts were made with the help of aerial photography. The large uncertainties which resulted from this technique were due to the very limited amount of images, often taken at a very irregular time interval. Moreover, knowledge of the connection between the visualisation of the process in an image and the underlying topography was still limited.

More structural coastal research, using nearshore exposures, started during the 1980s at the Coastal Imaging Lab of Oregon State University (USA). Holman and Sallenger (1986) started to use time averaged video images, which was an important breakthrough. The black and white time exposure images showed bright intensity patterns reflecting the areas where incident waves preferably break. This allowed for detection of morphological features and determination of their cross-shore and longshore length scales. By mapping underlying morphology from time exposure images they proved that video imaging could be an attractive and useful tool for coastal research.

In continuation of this, the ARGUS research program was started in 1992 by the Coastal Imaging Lab (Holman, 1994), with the installation of the first fully autonomous video recording system at the beach of Yaquina Head, Oregon, USA.

2.2 The ARGUS program

The first generation of techniques was ‘hand driven’ and data were stored on video tapes. However, since 1992 and the start of the Argus program, cameras have been installed whose data collection has been computerised and recorded images are stored on the hard disk of a computer. The present day there are over 10 fully automated Argus stations operating at different beach locations around the world.

An Argus station consists of one or more video cameras attached to a point high above the beach. Each camera views obliquely along a (part of the) beach and is connected to a computer where the images are being processed. Every (daylight) hour data are gathered, comprising three different sorts of pictures:

- a snap shot image, which is a ‘normal’ picture

- a time exposure image, which is an averaged image of 1200 snap shots, recorded every 0.5 second during a period of 10 minutes
- a variance image, also called a standard deviation image, indicating locations of time changing image intensity



Figure 2.1 Snap shot image (left), Time averaged image (middle) and Variance image

The only image being used in this study is the time exposure image. The 10 minutes timescale has been chosen such that it averages sufficiently over the wave frequencies that occur in the surfzone, while at the same time, steady wave conditions can be assumed.

Until recently all Argus stations were initially installed for research purposes. The Argus station 'Jan van Speijk' at Egmond aan Zee and the Australian site at the Gold Coast are the first sites primarily installed for coastal management. More information can be found in the report Argus & Kustbeheer (Aarninkhof, 1999).

Once a day, the data gathered at most Argus sites is being downloaded to Oregon where they are added to the central Argus database at the server of the Coastal Imaging Lab. The data is accessible via the internet at www.oce.orst.edu:8080. For people interested in the Dutch sites, it is worth visiting www.wldelft.nl/argus.

2.3 Image processing

2.3.1 Introduction

Before the information of an image can be used for coastal studies it is important to take into account some photogrammetric techniques. At first the coordinates of all pixels in the image have to be transformed to real world coordinates in order to find the real position of a certain feature observed in the image. The derivation of the equations used for rectification of an oblique image is presented after Lippmann and Holman (1989). Beside this, some considerations have to be made with regard to image quantification and pixel resolution.

2.3.2 The rectification process

Rectification means the transformation from image coordinates to real world coordinates. Images are two-dimensional whereas the real world is three dimensional. This means the equations for the rectification process are only fully defined when transforming real world coordinates to image coordinates and not the other way around. In that case one ground coordinate has to be known. Since we are interested in processes occurring at the water surface, the problem is solved by assuming that the z-coordinate in the whole nearshore

zone is equal to the sea level. The errors in the transformation, occurring from the moving watersurface (of the order of the wave amplitude) are assumed negligible compared to the height of the camera. For the Argus site 'Jan van Speijk' (camera height of 43 m) the errors in the transformation are smaller than 2 %.

The conventions as used in Argus image transformation are shown in Figure 2.2.

Here, image coordinates, located in the focal plane, are denoted with small letters (x,y), while for the coordinates in the ground plane capital letters (X,Y) are being used. The optic centre of the camera is located at point O, at a distance Z_c above the ground plane. The other parameters are:

- N = Nadir : the vertical projection of O on the ground plane. It is the origin of the ground coordinate system
- Nadir line : line connecting O and N
- f_c = focal length : distance between the focal plane and O
- p : centre of the focal plane (principal point)
- P : centre of the ground plane
- principal line : bisection line of the focal respectively ground plane
- optic axis : axis through O, p and P
- τ = camera tilt : angle between the optic axis and the nadir line
- q and Q : location of any point in the focal and ground plane respectively

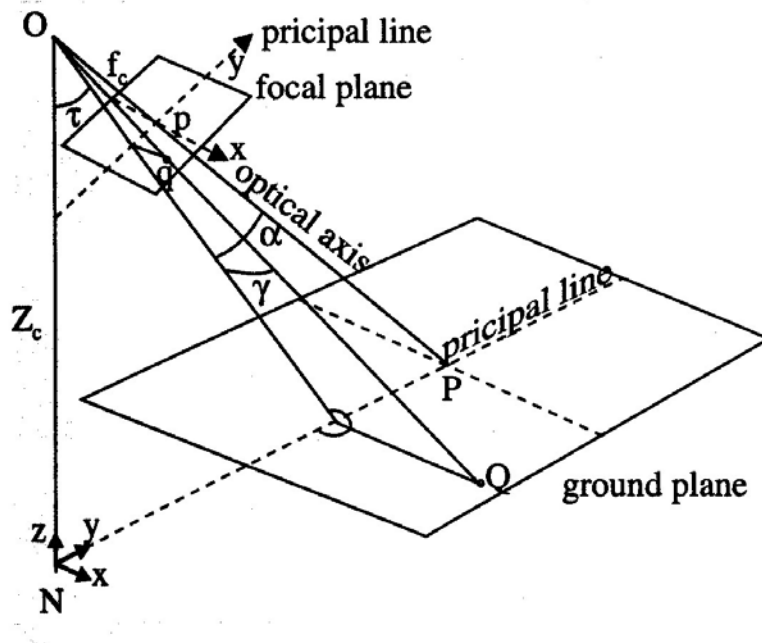


Figure 2.2 Conventions in Argus photogrammetry (Lippmann and Holman, 1989)

The ground coordinates $(X,Y)_Q$ can be derived directly from the image coordinates using the following relations:

$$X_Q = \frac{Z_c}{\cos(\tau - \alpha)} \cdot \tan \gamma \quad (2.1)$$

$$Y_Q = Z_c \tan(\tau - \alpha) \quad (2.2)$$

The angles α and γ , which determine the actual position in the ground plane with regard to the optic axis, are defined as:

$$\alpha = \arctan\left(\frac{y_q}{f_c}\right) \quad (2.3)$$

$$\gamma = \arctan\left(\frac{x_q}{\sqrt{f_c^2 + y_q^2}}\right) \quad (2.4)$$

However, when applying these expressions there are a few difficulties. One of the problems is the determination of the camera tilt τ and the focal length f_c , both are hard to measure or estimate.

For the focal length the problem is solved by counting pixels from the screen and relate them to the field of view of the camera. To do this the following expression can be used:

$$f_c = \frac{x_e}{\tan\left(\frac{\delta}{2}\right)} \quad (2.5)$$

where x_e represents the measured distance from the principal point p to the right-hand edge of the image and δ the field of view of the camera. Nevertheless, this method introduces the field of view of the camera δ , which is also hard to measure in the field.

The other problem considers the definition of the coordinate system. All cameras are aimed in such a way, giving the best possible view of the nearshore. This results in a coordinate system which does not correspond with the more practical and generally used coordinate system, where the axes are shore-normal (X-axis) and -parallel (Y-axis). The necessary angle of rotation between the two coordinate systems ϕ and also the camera roll θ , which is the angle between the camera relative to the horizon, are both parameters which can also not be measured accurately in the field.

Thus, before an oblique image can be projected onto a horizontal plane with a certain z -level (rectification), four parameters have to be solved: δ , τ , ϕ and θ . Determination of these parameters in the rectification process requires so-called Ground Control Points or GCP's. The GCP's are fixed objects in the field of view of the camera from which the exact location is known.

By also knowing the image coordinates of a GCP, equation (2.1) and (2.2) give two relationships between image coordinates and ground coordinates. So, to solve all four unknown parameters at least two GCP's are necessary. For optimization of the solution often more than two GCP's are being used. When done accurately, the errors are about 0.25° for τ , 0.5° for ϕ and 1 % for f_c (Lippmann and Holman, 1989). These kind of errors are subpixel and therefore smaller than the error in pixel resolution (see section 2.3.3).

2.3.3 Pixel resolution

An Argus image is a digitised image, this means it consists of 640 x 480 (NTSC) or 768 x 576 (PAL) pixels in which all the image information is stored. The pixel resolution is defined as the real world distance (Δx or Δy) which is covered by one pixel in the rectified image.

Each pixel of a digitised image represents a small part $\Delta\delta$ of the overall camera field of view δ , which for example is approximately 29° for one of the outer cameras at the 'Jan van Speijk' Argus site (see table 2.1). The Egmond Argus station has PAL cameras, therefore the width of the image is 768 pixels meaning $\Delta\delta$ is $29/768 = 0.038^\circ$ per pixel. With this value the pixel resolution can be calculated. Considering a ground coordinate system with the x-axis shore normal and the y-axis parallel to the shore, the estimated longshore- (Δy) and cross-shore (Δx) camera resolutions are:

$$\Delta x = R \cdot \sin(\Delta\delta) = R \cdot \Delta\delta \quad (2.6)$$

$$\Delta y = \frac{R \cdot \Delta\delta}{\cos(\tau - \alpha)} \quad (2.7)$$

where R is the straight distance from ground location to camera. So, the pixel resolution strongly depends on the position on the screen (or, equivalent, on the position of an object in the ground plane). Figure 2.3 shows some values of cross-shore and longshore pixel resolution. On both figures the x-axis is the longshore axis, the y-axis the cross-shore axis. The five parts in which the figures are divided represent the fields of view of each camera. The location of the cameras can be found around (-100,-100). Clearly the values of pixel resolution increase with increasing distance from the cameras.

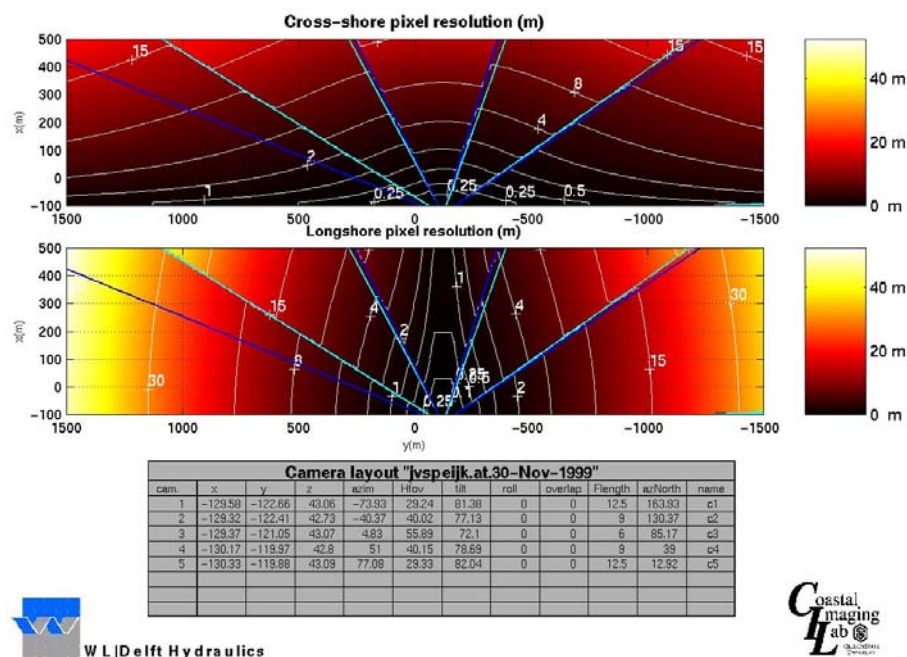


Figure 2.3 Pixel resolution for Argus station JV Speijk

2.4 Egmond site 'Jan van Speijk'

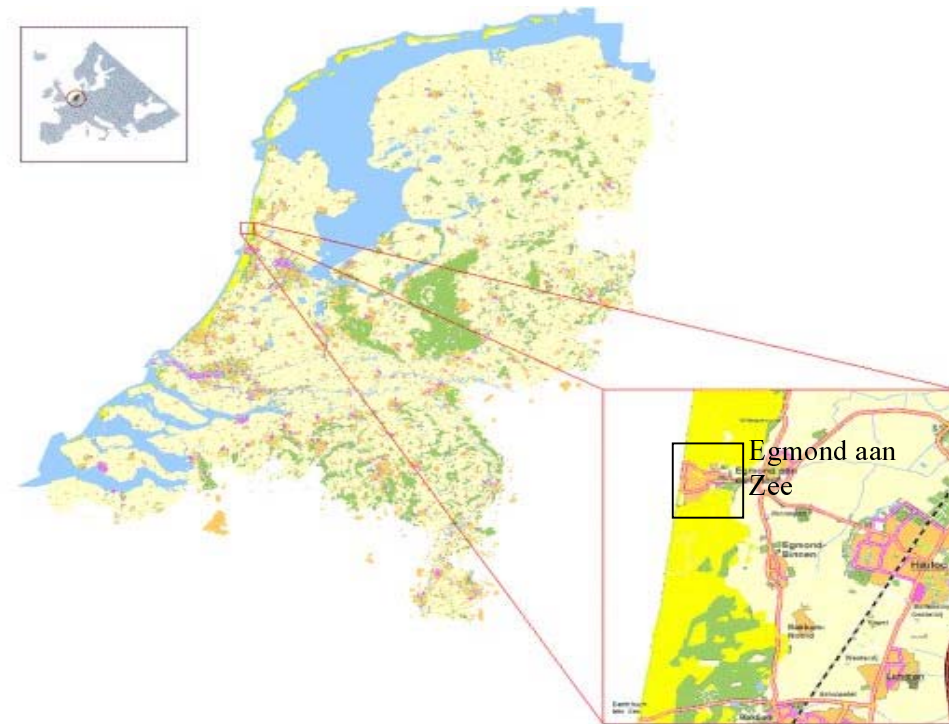


Figure 2.4 Location study area

The study in this report is based on the images from the Argus site 'Jan van Speijk' located at Egmond aan Zee, a village at the Dutch coast in the province North Holland. Here at the top of the lighthouse, named after the Dutch naval hero 'Jan van Speijk', the third Dutch Argus site became operational in May 1999. The installation was done by Delft Hydraulics in assignment of Rijkswaterstaat Directie Noord-Holland. Five cameras are installed, each monitoring a different part of the beach. Together they cover a full 180 ° field of view on the Egmond beach around the lighthouse.



Figure 2.5 Argus cameras on top of the lighthouse 'Jan van Speijk'

For this station, a local coordinate system has been defined. The origin is located within a meter away from the main RSP pole of transect 38.00, at the RD-coordinates $x = 103011$ and $y = 514782$. The y-axis is parallel to the shore and positive to the south, the x-axis is cross-shore and perpendicular to the y-axis. Its direction is positive in seaward direction and orientated at 278° from the north.

The camera station itself is located on top of the lighthouse at almost 43 m above NAP. The table beneath gives some information about the cameras and lenses.

Station	Camera	Camera.id	Orientation	Focal distance	Horizontal field of view
JVS0S	c1	JV01C	N	12 mm	29°
	c2	JV02C	NW	9 mm	39°
	c3	JV03C	W	6 mm	55°
	c4	JV04C	ZW	9 mm	39°
	c5	JV05C	Z	12 mm	29°

Table 2.1 Camera information Argus site 'Jan van Speijk'

Before rectifying the image, the relationship between screen and field coordinates has to be established correctly by using at least two GCP's. This is called: 'doing the geometry'. GCP's are available for all the cameras at the 'Jan van Speijk' Argus station. So, for each camera the so-called 'geometry' can be defined. If, for some reason, a camera changes position, the old geometry solution is not valid anymore and a new one must be made. This is why the geometry must be checked on a regular base, especially when the images are being used for model purposes.

2.5 Standard post-processing tools

Since the start of the Argus program the video images from multiple Argus stations have been used for coastal research. This resulted, depending on the research goals, in all sorts of image analyses techniques. In continuation of this and especially within the framework of Argus for coastal management some interesting and useful post-processing tools have been developed (Aarninkhof, 1999) which are also used in this study. The most important ones are described below, these are:

- The Argus Merge Tool:

This application automatically makes so called 'composition images' or 'merged images'. Single time averaged Argus images are being rectified and joined together. This results in a planview of the nearshore zone. Figure 2.6 shows an example of merged images.



Figure 2.6 Merged images for Argus station 'Jan van Speijk'

The camera location is located at the bottom of the image near $x = -100$ m. It shows a planview covering 3000 m longshore and more than 800 m cross-shore.

The bright regions indicate regions of intense wave breaking hence the location of shallow water depth. In this way morphologic features like the coastline (waterline) and longshore breaker bars can easily be identified and their behaviour can be monitored over time. In figure 2.6, four breaker bars can be identified. This includes the shoreface nourishment near $y = 700$ m.

- Argus Stack Tool

The Argus stack tool automatically creates so called 'stacked images'. These images are created by collecting the image intensities along one transect at one tidal level. The movement of the dissipation patterns in time enables a quantitative impression of morphologic changes for that transect.

Figure 2.7 shows an example of a stacked image processed from the 1st of June 1999 to the 15th of June 2000. This image indicates the dissipation pattern along the cross-shore transect at $Y = -50$ m for $Z_{\text{tide}} = 0$ NAP. At this location sand bar movement in time is clearly visible.

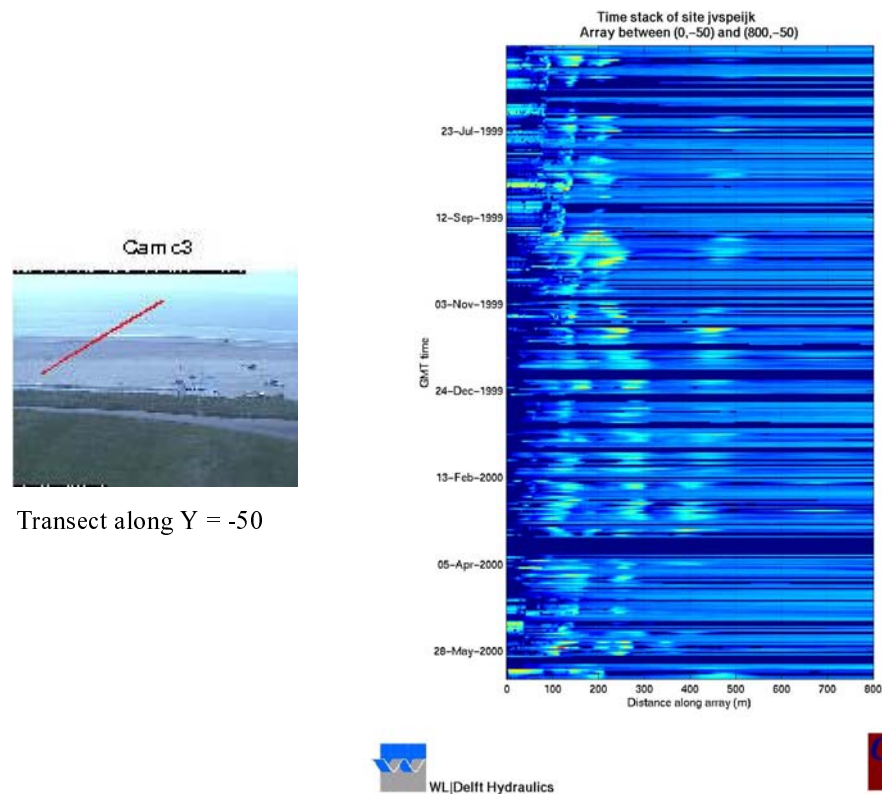


Figure 2.7 Stacked images for transect $y = -50$ m

Next is the most important Argus image analysing technique for this study.

- The waterline Detection Technique (Aarninkhof and Roelvink, 1999).

This technique makes use of color differences between wet and dry pixels in an Argus image to identify the horizontal waterline. In combination with hydrodynamic modelling of the vertical elevation of the waterline, the location of the waterline is known in three-dimensional space.

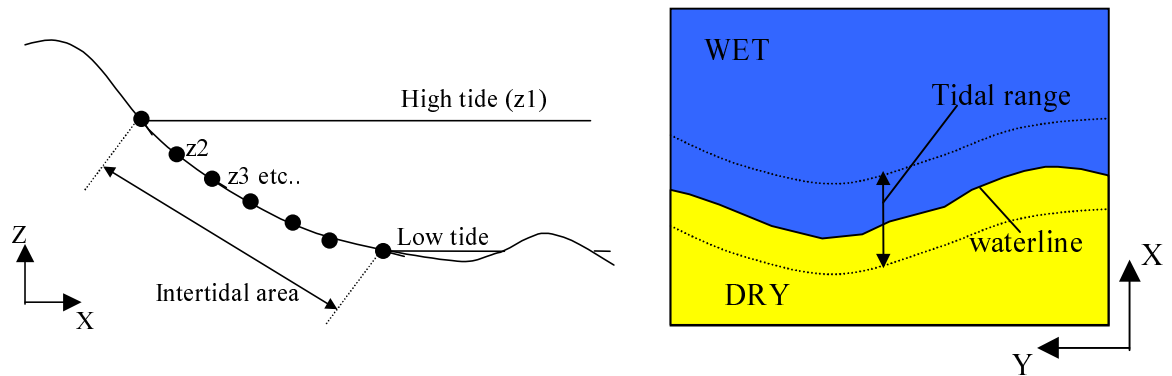


Figure 2.8 Principle of the waterline detection technique, view on profile (left) and top view (right)

Modelling multiple waterlines throughout one tidal cycle makes it possible to create intertidal beach profiles (see Figure 2.8). In this way the morphodynamics of the intertidal beach can be determined.

A schematic overview about the working of the waterline detection model is shown in Figure 2.9. More about the working and validation of this technique will be treated in the following chapters.

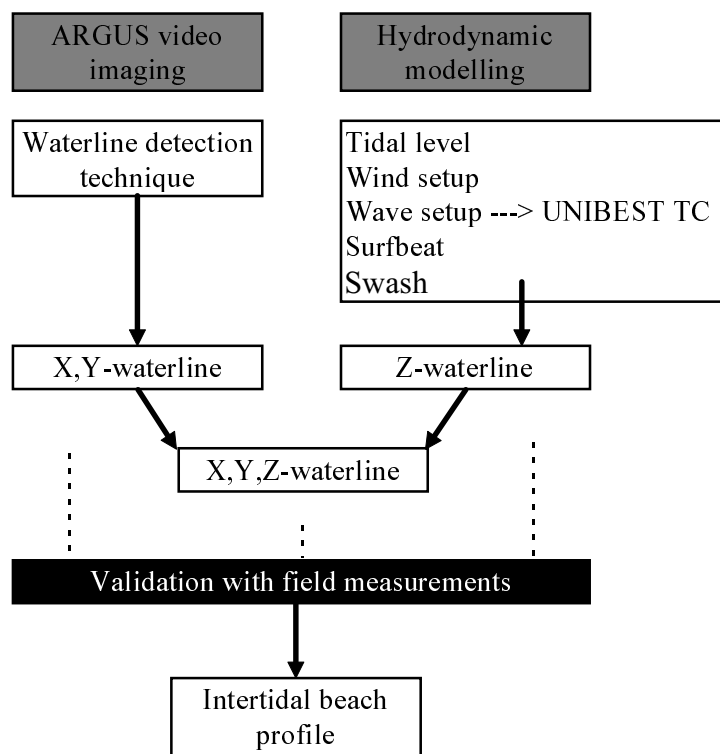


Figure 2.9 Schematic overview waterline detection model

3 Waterline detection model

3.1 Introduction

In order to determine the location of the waterline it is necessary to find the horizontal position of the waterline from time-averaged Argus images (X,Y-coordinates) and to make a good estimation of the accompanying elevation from hydrodynamic measurements (Z-coordinates). In such a way, the waterline on a beach is known in three dimensional space. Since every hour a new Argus image is available, the same operation can be done multiple times within a tidal cycle (Fig. 2.8). Putting these waterlines together creates a three dimensional intertidal beach surface (Fig 2.8).

In recent history several researchers worked at the development of waterline detection techniques capable of predicting the location of the waterline. Considering the scope of this study, two of such image analysing techniques are particularly relevant. These techniques are briefly mentioned below and a summary is given in Appendix A.

Plant and Holman (1997) adopt the visually observed location of the shoreline break as an indicator for the horizontal waterline, while the associated water depth is estimated empirically as a function of the hydrodynamic regime at the shoreline. Janssen (1997) identifies the waterline from a cross-shore correlation analysis between the cross-shore image intensity profile and the variance profile. However, in absence of a well-pronounced shoreline break, the method of Plant and Holman could often not be applied to the Dutch beaches, while the variance method of Janssen turned out to be complicated to apply. Colour images, introduced in 1997, created new perspectives.

The technique used in this study for finding the horizontal (X,Y) coordinates of the waterline is based on the waterline detection method after Aarninkhof and Roelvink (1999). In their method they use color differences between ‘wet’ and ‘dry’ pixels to estimate the horizontal location of the waterline. Within an Argus image a region of interest, with both ‘dry’ and ‘wet’ pixels, is determined. Information from each individual pixel is then collected and categorised on the basis of color. This categorisation leads to a histogram with two clusters of pixels, one includes the pixels on the mainly dry beach and the other one pixels on the mainly wet beach. This determines the transition between dry and wet and therefore the location of the waterline.

In the same year, the waterline detection method has been improved and a first validation has been made with Egmond Coast3D bottom data (Aarninkhof and van Kessel, 1999). Despite the fact that the validation dataset was not ideal it showed some promising results. The improved method was the starting model of this study.

The first part of this chapter explains how this method works, in other words, how color information from time exposure Argus images is used for finding horizontal waterline coordinates. The second part treats the method for finding the accompanying height, done by hydrodynamic modelling.

3.2 Determination of the X,Y-coordinates

The working of the waterline detection technique can be divided into three steps:

1. Pixel clustering based on color information and determination of the discriminator function.
2. Testing to what extend the clustered pixels are discriminated. If the discrimination is insufficient, the model goes back to step 1 and the pixels are clustered based on other colour information. If this is still insufficient, the image is being rejected.
3. Interpolation to waterline coordinates.

The following sub-paragraphs explain these three steps.

3.2.1 Pixel clustering based on color information

The waterline detection method makes use of the color information stored in Argus color images. Image intensities are defined in the RGB color space, this means that the color of each pixel in the image is defined as a mixture of red, green and blue (RGB). The value of each color varies between 0 and 1.

When the region of interest is defined (figure 3.1a), the pixel intensities are converted to the HSV ('Hue Saturation Value') color space. HSV color space separately treats the color information (by means of H and S) and the grayscale information (by means of V). The Hue values vary from 0 to 1.0, the corresponding colors vary from red ($H = 0$), through yellow, green ($H = 0.5$), cyan, blue, and magenta, back to red ($H = 1$ again). Saturation values also vary from 0 to 1.0, the corresponding colors vary from unsaturated (shades of gray) to fully saturated (no white component). This means the Saturation value is 1 for all the primary and secondary colors (red, green, blue, cyan, magenta, yellow) and 0 for black and white. Value, or brightness, varies from 0 to 1.0, where the corresponding colors become increasingly brighter.

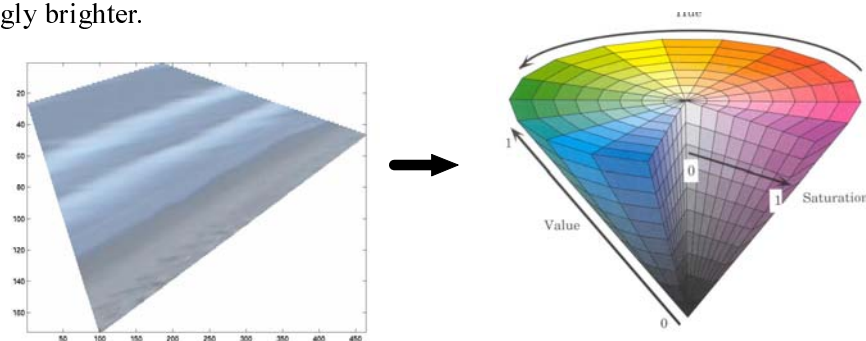


Figure 3.1 Conversion of image intensities to HSV colorspace

HSV and RGB intensities of multiple images from Argus station 'Jan van Speijk' have been investigated. This showed that some intensity combinations separate clusters of dry and wet pixels at different locations within that colorspace. The best results proved to be Hue-Saturation and Hue-Green combinations. The separation based on Hue-Saturation seems, in general, to work best. Especially for images which show calm weather conditions. A separation based on Hue-Green seems to work better for images that show rougher weather conditions (lots of wave dissipation ('white sea')) and also for cameras which are affected

by the weather (see section 3.2.4). Consequently both combinations are used in the model whereas the model always tests on Hue-Saturation first.

Figure 3.2 shows a histogram of pixel intensity data in the H-S space after the full data set has been scaled between 0 and 1.0.

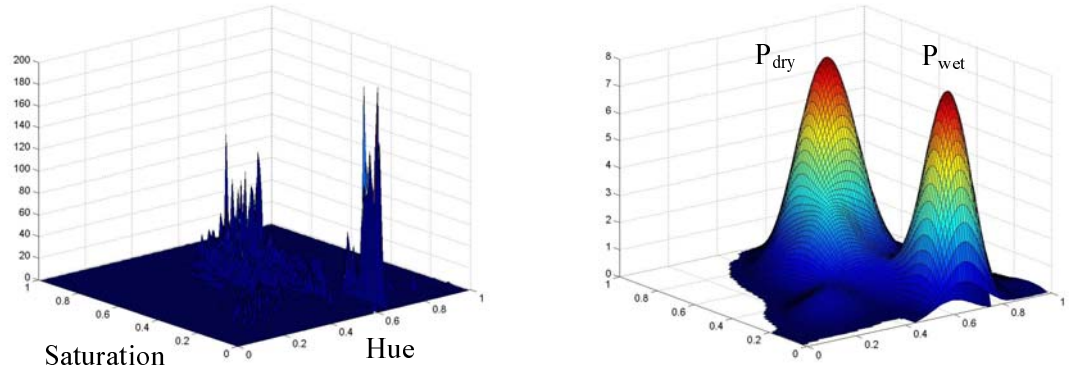


Figure 3.2 Clustering of dry and wet pixels, raw categorisation (left) and smoothed (right)

The key element now is to separate between the two clusters of pixels and to determine a discriminator function. First the histogram is smoothed by a Gaussian-shaped filter until two uniquely defined peaks (P_{dry} and P_{wet}) are left (Figure 3.2b). Introducing the line l as the line between the two peaks, the first order discriminator m_1 is defined as the line perpendicular to the line l crossing the location of minimum probability of occurrence along l .

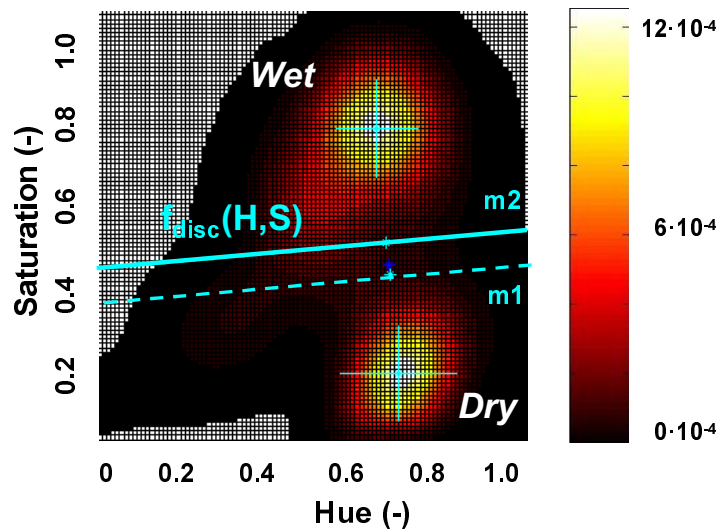


Figure 3.3 Determination discriminator function dry/wet cluster of pixels

Important here is that the smoothing operation introduces an artificial off-set of the location of minimum probability of occurrence. When smoothed, the location of minimum probability tends to move towards the cluster with the smaller total number of occurrences $N_{tot,small}$. In figure 3.4 the problem is explained for the one dimensional case.

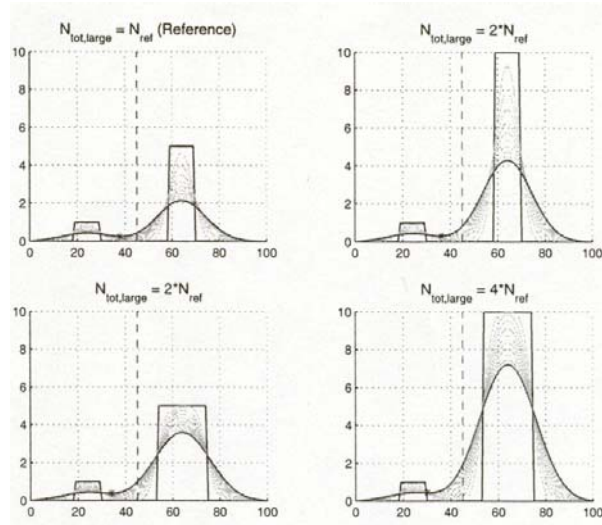


Figure 3.4 Effect of smoothing on location of minimum probability of occurrence

The magnitude of the artificially introduced shift dS increases with an increase of the ratio $N_{tot,large}/N_{tot,small}$, as well as with an increase of the number of smoothing steps N_{smooth} . The empirical relationship to correct for this effect reads:

$$dS = f_{sign} \cdot \left(\frac{N_{smooth}}{N_{smooth,max}} \cdot \frac{N_{tot,small}}{N_{tot,small} + N_{tot,large}} \right) \cdot dS_{max} \quad (3.1)$$

where f_{sign} is a sign function that arranges the shift to be in the right direction, $N_{smooth,max}$ is the maximum number of smoothing steps allowed and dS_{max} the maximum shift allowed, which is defined relative to the absolute distance between the peaks P_{dry} and P_{wet} of the two clusters. The value of dS_{max} could vary for different Argus sites. By simply testing and comparing model solutions it is easy to set this parameter at a best possible value, which may vary between reasonable limits without changing model results. After the correction for the smoothing-induced shift, the line m_2 is the new discriminator line, mathematically prescribed as:

$$S = p_1 \cdot H + p_2 \quad (3.2)$$

Now, the two-dimensional discriminator function $f_{disc}(H,S)$ is defined as:

$$f_{disc}(H,S) = p_1 \cdot H + p_2 - S \quad (3.3)$$

The discriminator function returns values zero when a combination of H and S respectively H and G is on the line m_2 , it returns negative values in the wet area and positive in the dry region. Based on this principle, each pixel can be categorised depending on the sign of f_{disc} .

The categorisation of the image pixels within the region of interest can now be translated into a binary image, where black spots represent negative values of f_{disc} (hence wet areas) and white areas the positive values (indicating dry beach). The first picture of figure 3.5 shows this binary image. In the next picture, the raw categorisation is corrected by requiring spatial consistency. This means that wet pixels surrounded by dry ones become dry and vice

versa. The image coordinates of the waterline can now be determined by using an edge detecting technique, which determines the location of the pixels on the boundary between black and white (wet and dry). This leads to the last picture of figure 3.5.

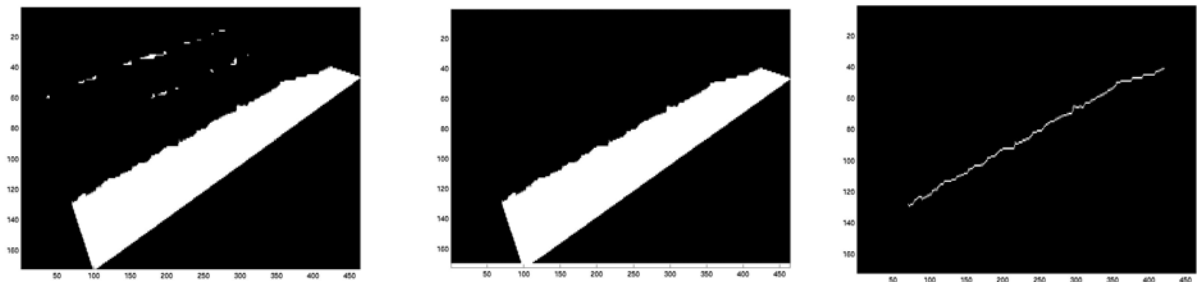


Figure 3.5 Successive steps to determine the image coordinates of the waterline

3.2.2 Testing the discrimination of pixels:

Not all time averaged images are useful for the waterline detection method. Therefore, it is important to use criteria to automatically test the applicability of an image.

The applicability of one single Argus image is being tested based on the discrimination capacity between dry and wet beach. This is done by using statistics derived from the values in the Hue/Saturation (or Hue-Green) histogram. On the base of these statistics, the image is being tested on two criteria. If one of the criteria satisfies the model accepts the image for further application. The criteria are:

- Criterion 1: Two, sufficiently discriminated, pronounced clusters of pixels.

This criterion requires the amount of observations in both clusters to be of the same order. It is set such that both clusters need to comprise a minimum of 30 % of the total amount of observations. To test to what extent the clusters are discriminated it is set that the standard deviation of both clusters must be smaller than 1.2 times the distance between the top of the cluster and the point of minimum probability of occurrence in the histogram. This is to guarantee that both clusters are well-pronounced. When both conditions are valid, criterion 1 satisfies, the model will not test on criterion 2.

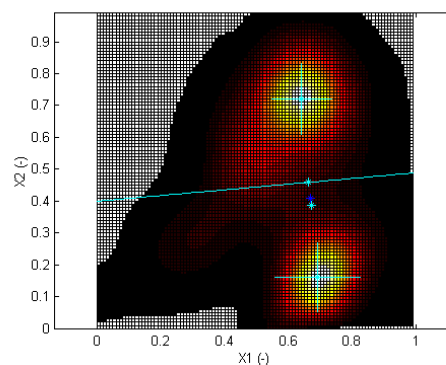


Figure 3.6 Standard deviations of the clusters in respect to the discriminator line

- **Criterion2:** Two clusters of different size, but well discriminated.

When only a small part of the area of interest is wet or dry there can be two clusters of different size. In this case the two clusters can still be strongly discriminated. Quantitatively this means that one of the clusters comprises less than 30 % of the total amount of observations. Because of this, the discrimination condition has become a bit more strict: the standard deviation of both clusters must be smaller than 0.9 times the distance between the top of the cluster and the point of minimum probability of occurrence in the histogram.

Images which do not meet these criteria are automatically rejected and no solution can be found using the Hue-Saturation color information. When that happens the model goes back to the starting point and tries other color information. This means that the same procedure of clustering of pixels and testing on the two criteria is now carried out for Hue-green colour information. When again no solution can be found the image is definitively rejected.

3.2.3 Interpolation to waterline coordinates

Application of the discriminator function f_{disc} on the image of interest results into a binary image indicating dry and wet pixels (section 3.2.1). First the waterline image coordinates are translated into field coordinates. Next, the interpolation to waterline coordinates is being carried out in terms of these field coordinates. Because the model identifies multiple transition points between wet and dry in the swash zone it is then possible to average multiple observations within the swash zone.

Next, the individual observations are connected based on a 'nearest-neighbour' criterion. To make sure the jump to the next observation is not too big, it is set that the jump may not be bigger than 1.2 times the longshore pixelresolution at that location. In case of bigger jumps the waterline is divided into individual parts. To accept a part, it has to cover a minimum of 20 % of the longshore length within the region of interest or it must be composed out of a minimum of 150 individual observations. The result is a series of swash averaged waterline field coordinates, a line through these points represents (a part of) the waterline within the region of interest in terms of field coordinates.

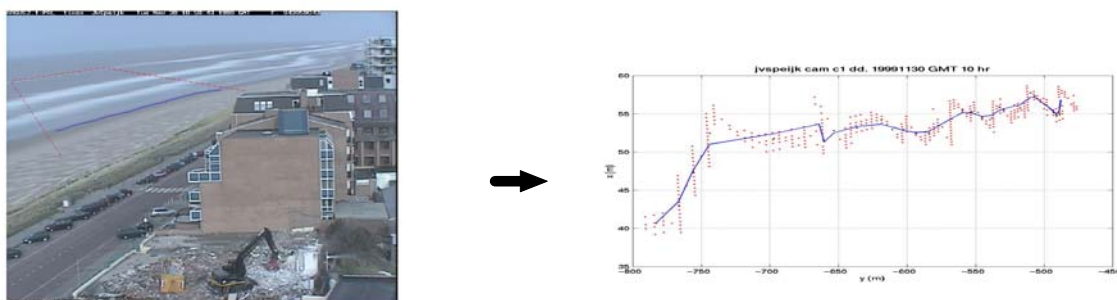


Figure 3.7 Translation of the waterline from image coordinates to field coordinates

Figure 3.7a shows the waterline image coordinates as they were found by the edge detecting technique. The scattered points in figure 3.7b show the same coordinates in terms of field coordinates (an increase in pixel resolution causes an increase in scattered field coordinates). The solid line through the scatter is the eventual waterline after averaging over the swash zone.

3.2.4 Evaluation waterline detection technique

The most important information stored in an Argus image with respect to the waterline detection model is its color information. In particular the color differences between dry and wet areas. An extensive search through the 'Jan van Speijk' database indicates that these colors vary with the meteorological conditions. The most affecting ones are mentioned below:

- The most obvious color determining factor is the weather. Rough circumstances with a lot of wind and waves increase dissipation and the sea turns more white. Also the 'cloudiness' plays an important role, images are darker (gray) for cloudy or rainy weather. Morning fog or hazy weather cause the images to be more vague, often the images get white or light gray when further away from the camera.
- Colors also change due to differences in light during the day. For example morning light differs from the light in the afternoon and differs from light in the beginning of the evening.
- Another aspect, clearly visible on some of the 'Jan van Speijk' images, is some sort of blue haze caused by the camera itself. The cameras which are orientated south and south-west show this effect and probably need maintenance.

Other aspects which are suspected to be of influence on the colors are: the amount of alga in the water (seasonal aspect), nourishment's (depending on where the nourished sand came from), the glare of sunlight in the water and the shadows of buildings on the beach (causing local dark areas).

The observations described above cause the large variety of color information that can be found in an Argus image. Beside meteorological conditions also some site dependent factors can be found.

After testing and studying the applicability of the model in respect to these factors, 8 cases were found where the model can go wrong. These cases are shown in appendix B and will be treated below:

Case 1: Wet areas on the beach during falling tide

During the days of the field measurements, the weather was rainy and windy. These conditions can cause large wet areas on the beach at locations outside the swash zone. Looking at the example in appendix B, there is enough color information and it looks like the correct waterline has been found. Nevertheless, the calculated waterline is not the right one. It shows the outer edge of the wet areas and not a line in the swash zone.

Case 2: Moisture behind the Argus camera lens

Moisture makes the image vague and foggy and the extent of misting up the lens can cause changes in color. These effects can 'confuse' the model by mixing up dry and wet areas, resulting in the wrong waterline.

Case 3: Shadows on the beach

In the morning when the sun is low, the high buildings on the boulevard and also the higher dunes can cause shadows on the beach. These shadows darken parts of the beach and give the wrong color information to the model. In the example the waterline is detected in the left corner of the beach, fully provoked by the shadows.

Case 4: Glare of sunlight in the water

Looking at the example, the sea colors white at one corner and much darker in the opposite corner. This effect, caused by the sun reflecting on the water, makes the darkest part of the

sea part of the cluster of pixels representing land. The result is a modelled waterline 'cutting' off a part of the sea.

Case 5: Rain

When it rains and especially when the wind is blowing straight into the lens, the camera lens is covered with rain drops. These rain drops change the color information of the pixels underneath, especially important at the intersection of land and sea. In the example the color information indicating land and sea is reversed, forcing the modelled waterline in the sea.

Case 6: Too far away or hazy weather

The areas too far away (+/- >600 m) often show a decrease in clearly distinguishable color information. The modelled waterline often deviates too much and can not be considered accurate enough. This effect, of course, depends strongly on the weather circumstances.

Case 7: People on the beach

This good example of a nice hot summer day at the Dutch coast shows the effect of sun-worshippers. They disturb the normally monochrome beach making it hard to find the waterline.

Case 8: Too dark

When it is too early in the morning or too late in the afternoon the twilight makes it difficult to use color information for detecting the waterline. This effect is already noticeable in the beginning of the twilight. Discrimination between dry and wet is probably still possible when using black-and white (Value) information.

It must be said that these cases do not always lead to wrong modelling. Most of such images are either rejected by the statistical model criteria or the result is (just) not affected by the disturbing factors. Nevertheless, a wrong waterline might be modelled. If such a waterline is part of a series of waterlines it can be enough to completely disrupt modelling of intertidal beach profiles. An additional check on temporal consistency of the modelled waterlines might partly solve for these problems, but is however not operational yet.

A clear advantage however is the high resolution of images in time. Every (daylight) hour of every day Argus images are recorded and stored. This means the user can choose which images (which hour(s) and day(s)) he wants to use for modelling purposes. Especially when interested in behaviour on a morphological timescale, like intertidal beach development, it is easy to run the waterline detection technique for only good weather circumstances. This approach will eliminate most of the problems.

For all other cases or unexpected events the model needs a user defined decision whether or not a computed waterline is valid. This implies that the waterline detection technique for finding the horizontal waterline coordinates can not be automated.

3.3 Modelling the Z-coordinate

When modelling the horizontal waterline from a time averaged Argus image it is assumed that all the X,Y-waterline points from that image have the same Z-coordinate. To find the accompanying Z-coordinate the method of Janssen (1997) has been adopted in this study. He initially defines the Z-coordinate as an addition of five components:

1. The measured waterlevel offshore
2. Wave setup
3. Wind setup
4. Swash (run-up and run-down)
5. Surfbeat

Addition of the first three terms represents the average steady Z-level of the waterline, the other two are the dynamic fluctuations around this level.

The following sections describe these five components and their contribution to and implementation in the model.

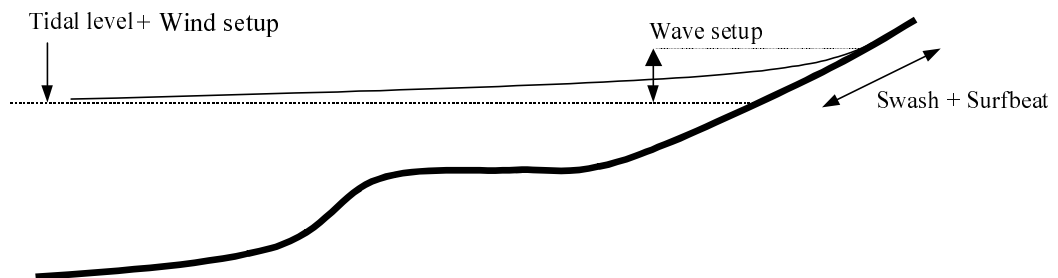


Figure 3.8 Determination of the waterline height

3.3.1 The measured waterlevel offshore

Starting point for determination of the Z-coordinate are the measured waterlevels from the wavec and waverider buoys located offshore the harbour entrance of IJmuiden. The distance between IJmuiden and Egmond is about 18 kilometers, causing an approximate tidal lag of 20 minutes. This means the waverider data can not be used directly for modelling the waterlevel at Egmond.

To solve this, the model makes use of tidal information from IJmuiden and Petten gathered from the tidal generator (Rijksinstituut voor Kust en Zee (RIKZ)), which is capable of calculating the astronomical tide. Because Egmond is located just in between of IJmuiden and Petten, the astronomical tide in Egmond can be estimated as the average line between the two tidal curves.

Next, the waterlevel measurements at IJmuiden are used to determine the difference between the astronomical tide and the real waterlevels. The differences between the measurements and the astronomical data from the generator at IJmuiden are assumed to be the same for Egmond. Adding this difference with the averaged astronomical tide results in the waterlevel values used in the model.

In a formula this reads:

$$z_{tide,Egm} = \frac{z_{astr,IJm} + z_{astr,Pet}}{2} + (z_{measured,IJm} - z_{astr,IJm}) \quad (3.4)$$

The time averaged images cover a time span of 10 minutes, consequently the resolution in time of the waterlevel dataset is also 10 minutes.

Last remark concerns the fact that in the near future this method will probably be replaced by direct waterlevel measurements at Egmond. Tidal gauges which are already situated in Egmond are expected to become operational in July 2000. The tide and wave information from these gauges will be of use for checking other model aspects, like the calculation of the wave setup with Unibest.

3.3.2 The wave setup using UNIBEST-TC

A part of the variation in mean nearshore water level is a function of the incoming wave field. From the breaking point the mean water surface slopes upward to the point of intersection with the shore. The wave setup is defined as that superelevation of the mean water level caused by wave action alone (Shore Protection Manual, 1984).

For calculations of the wave setup, the model uses the Unibest wave module. This section describes this module only in concept, the rest can be found in Appendix C.1 which originates from: UNIBEST-TC 2.0, Overview of model formulations, WL | delft hydraulics, October 1997.

The wave propagation model consists of three first-order differential equations, viz. the time averaged wave energy balance (Battjes and Janssen, 1978), the balance equation for the energy contained in surface rollers in breaking waves (Nairn et al., 1990) and the horizontal momentum balance from which the mean water level set-up is computed. The refraction of the waves is computed using Snel's law. The three coupled equations can be solved by numerical integration over the cross-shore profile.

To solve the three coupled equations, boundary conditions are necessary. One of these boundary conditions is a bottom profile. The ideal situation for the input of a bottom profile would be a measured bathymetry. Because such measurements are not available for every day at every location at Egmond and due to the fact that the Egmond beach is subject to relatively fast morphologic changes, a synthetic bottom profile has to be used.

Janssen (1997) compared Unibest wave setup results with setup measurements for three different bottom profiles: an equilibrium profile (Bruun, 1954), a linear profile and a real/linear profile (figure 3.9). The last one being a linearisation of the real Noordwijk (Dutch coast near Egmond) bathymetry. From approximately $Z = \text{NAP} - 5 \text{ m}$ all three profiles go to $\text{NAP} - 18 \text{ m}$ by linear interpolation.

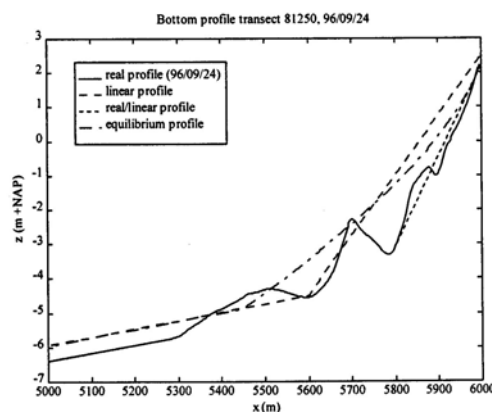


Figure 3.9 Tested bottom profiles according to Janssen, 1997

By comparing wave setup model results with wave setup measurements (at the waterline) he calculated the root mean square error ε_{rms} of these differences for each profile for 21 testcases. The best results were found for the equilibrium profile, the rms errors amounted 0.0197 for low tide, 0.0085 for mid tide and 0.0159 for the high tide situation. In a formula this reads:

$$\varepsilon_{rms} = \sqrt{\frac{\sum_{i=1}^N (\eta_i - \eta_r)^2}{N}} \quad (3.8)$$

η_i = calculated wave setup at the waterline for one of the synthetic bottom profiles, subscript i indicates one of the 21 testcases.

η_r = calculated wave setup in reality

N = number of considered cases.

The theory of an equilibrium beach profile states that because of a constantly changing wave field this profile is never reached. There exists a sort of dynamic equilibrium in which over a long period of time the profiles are more or less the same (van der Velden, 1995). This study also concerns beach profile development over longer periods of time. The real Egmond profile is not known, this is why the equilibrium profile as an average estimation of the long term profile seems attractive in this respect.

For this reason and also based on Janssen's findings including the fact that the Noordwijk beach is very comparable with the beach at Egmond it is decided to use the equilibrium profile for the wave setup calculations in Unibest. In formula this reads:

$$h(y) = Ay^n \quad (3.9)$$

Bruun (1954) found $n = 2/3$. For A which depends on the grain size (Moore, 1982) the same value has been chosen as in Janssen (1997). According to a grain size in the Noordwijk region (between 210-250 μm) the value for A should be $0.11 \text{ m}^{1/3}$.

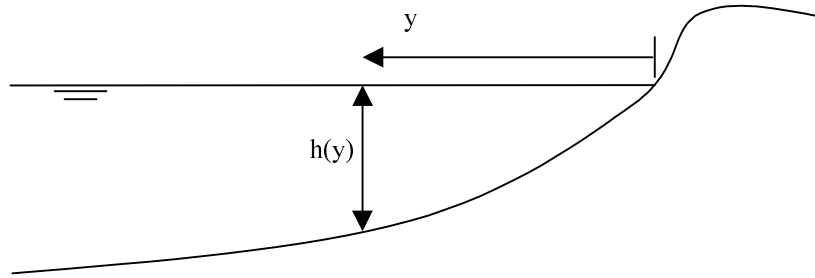


Figure 3.10 Definition sketch equilibrium profile

3.3.3 Wind setup

The friction between wind and water results in a force acting on the water. When the direction of the wind is shore normal or when a component of the wind direction is shore normal this force creates a rise in waterlevel at the coast.

The tidal levels used in the model are measured levels from a buoy located in the IJmuiden harbour entrance, this means that the biggest part of the total wind set-up is already included in these measurements. So only the distance between the buoy and the coastline

(in IJmuiden this is less than one kilometer) can be responsible for extra wind setup. Experience learns that this last kilometer of water does not create any significant extra set-up. Therefore the wind set-up can be ignored in the model.

3.3.4 Swash (run-up and run-down)

Run-up can be defined as the height above the still water level to which water from an incident wave will run up the face of a slope. In the opposite direction, below the still waterlevel this is called run-down. Swash is the generic term of both, the swash zone is therefore the area under influence of run-up and run-down.

When considering the waterline detection model it is assumed that the transition point between wet and dry is situated somewhere within the swash zone. It is therefore important to quantify the swash (height and length) in terms of wave and bottom characteristics.

Before the waves at Egmond reach the shore they travel over multiple breaker bars. This means that waves of considerable height are partly dissipated before reaching the beach causing swash. This is why the method used in the model starts with the assumption that only the waves able to pass the inner bar can cause swash. This approach is closely related to the one of Plant and Holman (1997) who state that the relevant wave height at the shore line is that which survives past the bar.

The calculation starts with an estimation of the inner bar height, in this study at NAP -0.5 m. The difference between the tidal level and the inner bar height determines the 'limited' depth. The waves able to pass this limited depth will break in front of the beach, they are responsible for swash. Thus:

$$h_{Lim} = z_{Tide} - h_{bar} \quad (3.10)$$

Consequently, at low tides when the inner bar is exposed ($h_{Lim} \leq 0$), the runup height is zero. For all cases where $h_{Lim} > 0$, the computation starts with a calculation of the breaker depth using linear wave theory. Appendix C.2 shows the iterative method for finding the breaker depth.

From the breaker depth, the breaker height can be determined (given a value for the breaking parameter). If waves of this height are able to pass the limited depth, swash is caused by these waves. Otherwise a new (lower) breaking wave height is determined, this one must be capable to pass the limited depth (see also appendix C.2)

Once the breaking wave height that causes swash has been found, the following formula is used to determine the swash height.

$$S_v = (2\xi_b - 0.4\xi_b^2)H_b \quad (3.11)$$

This formula has also been used by Janssen (1997) for his calculations of the wave setup. It is build out of two formulas: an expression for rundown height by Battjes and Roos (1974) who carried out runup measurements and an expression for runup by Hunt (1959), which introduces the Iribarren parameter ξ (appendix C.2)

3.3.5 Surfbeat

The term ‘surf beat’ was introduced by Munk (1949). With this term he refers to long waves being generated in the surf zone which act at the ‘beat’ frequency of wave groups. Later, Roelvink (1993) divides a system of waves into two characteristic time-scales: that of the individual waves and that of wave groups. Individual waves result in an approximately sinusoidal fluctuation of the water level and the velocity field, described above as swash. On the time-scale of wave groups there is a slow variation of the amplitudes of these fluctuations, this phenomenon is called surfbeat.

The combination of swash and surfbeat is causing the total dynamic fluctuations around the setup level.

Goda (1975) studied the variance spectra from offshore and nearshore wave measurements. He also found strong low frequency components in very shallow water. He defined surfbeat as the undulation of water surface with the frequency components between $f = 0$ and 0.05 Hz. By comparing surfbeat amplitudes with offshore wave amplitudes he derived an empirical relation, reading:

$$S_b = \frac{0.01H_{sig}}{\sqrt{\frac{H_{sig}}{L_0} \left(1 + \frac{h}{H_{sig}}\right)}} \quad (3.12)$$

The only interest in this study concerns the location of the waterline, this means the waterdepth is zero. The expression between brackets reduces to one and can be left out. As a result, the surfbeat height near the waterline only depends on deepwater wave data (H_{sig} and L_0).

3.3.6 The individual contribution of each component

The tidal measurements are close to the shore, this means wind setup can be ignored in the model. Therefore the computation of the vertical waterline coordinate is build out of 4 components. Starting point is the tidal level. Each of the components of wave setup, swash and surfbeat add something to that level to get the elevation of the waterline. Figure 3.11 shows the individual contribution of each of those components for different tidal levels and wave heights. The 18 cases represent the circumstances at the 29th and the 30th of November 1999 between GMT 09:00 and 16:00.

The inner bar gets exposed at lower tidal levels, consequently the swash height decreases for lower tidal levels. For cases 16,17 and 18 the swash is totally blocked. At the same time the values of swash, surfbeat and wave setup increase for bigger wave heights.

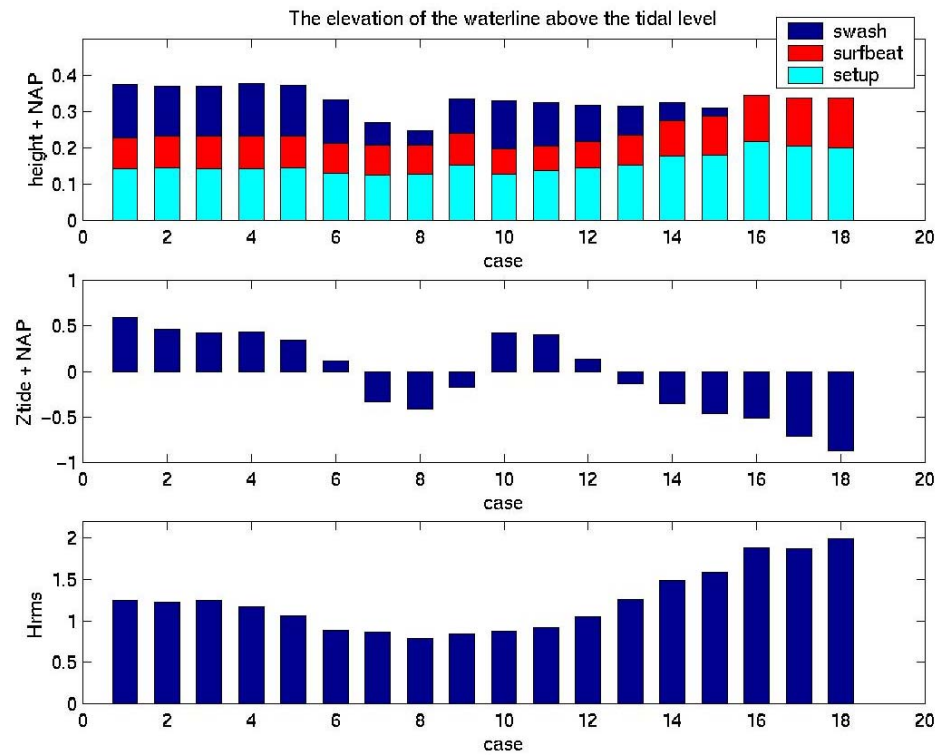


Figure 3.11 The individual contributions of wave setup, swash and surfbeat to the total waterline height

4 Model validation with field measurements

4.1 Introduction

Before this study, the waterline detection model was only roughly validated (Aarninkhof and van Kessel, 1999), using a relatively small dataset of useful coast3D bottom profiles. The results were promising but the availability of only bottom profiles did not make clear if deviations between model and measurements could be ascribed to inaccurate modelling of the horizontal location of the waterline (video-based detection model) or inaccurate modelling of the associated vertical elevation (or both). Besides, the Coast3D location was located far from the Argus camera, introducing relatively large errors. Consequently, for better determination of the model performance, there was still need for a dataset of waterlines (x,y and z coordinates) relatively close to the Argus camera with a high resolution in time and space.

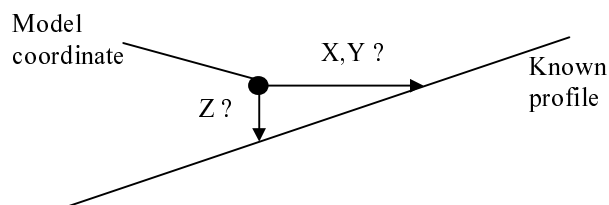


Figure 4.1 Possible deviation between a known bottom profile and a modelled waterline coordinate

Therefore it was decided to carry out field campaigns to gather a vast amount of field waterline measurements for an independent validation of on the one hand the waterline detection technique and on the other hand the vertical coordinate model. The field measurements have been carried out at the Egmond ‘Jan van Speijk’ Argus site at the 29th and 30th of November 1999 and in continuation of this a second field campaign on the 14th and 15th of March 2000.

The first paragraphs within this chapter describe the approach that has been used, the actual execution and the results of these measurements. From these results some important conclusions can be drawn about the applicability and interpretation of the waterline detection model. The rest of this chapter describes the validation of the waterline detection model. Waterline measurements are compared with model results to find the accuracy of the model.

4.2 Approach to field measurements

When running the Argus-based part of the waterline detection model it results in a set of coordinates, indicating the waterline in the local Argus X,Y-coordinate system. Time averaged images are being used, meaning that these computed coordinates represent a 10 minutes average unambiguous waterline. In reality the waterline within that interval is not a static never changing line, it's location also depends on dynamic features like swash and surfbeat. So before the measurements can start, one question has to be taken into account:

how to define the ‘real’ waterline? or in other words, which line can be considered as the waterline for the measurements?

After observation of the swash zone at location and the evaluation of some model results it was decided to define the waterline as the visible transition between glistening and non-glistening sand. This corresponds with a location at the higher parts of the swash zone. The most important reasons for this decision is that this transition is easy to detect and it's position is less variable than the runup from individual waves. Moreover, because this ‘line’ is so easy to detect with the eye (probably due to certain color differences) there is a considerable chance that the waterline detection technique finds the same waterline. In that case the measured waterline also represents the waterline that would be found by the technique.

The main activities during the campaigns were dual. The biggest part consisted of measuring the exact location of multiple waterlines during one tidal cycle, the other part were video recordings of the swash zone for determination of the swash zone statistics at different tidal levels.

The first part is necessary for validation of the waterline detection technique and the vertical coordinate, this means the waterline has to be measured in X,Y and Z coordinates. The swash zone statistics will point out where the modelled waterline is located in the swash zone.

For this occasion the ten minute time averaged video images were digitised at half hour intervals (normally one hour). For this site it means camera five and four (the cameras orientated S and S-W) record a time averaged image during the first 10 minutes of every half hour. After this, camera three (orientated W) records a ten minute average image. Camera two and one (orientated N-W and N) record the last 10 minutes of every half hour. At each time interval the measurements took place within the field of view of the running camera(s). This comes down to the following areas:

camera 5 and 4 : measurements between $Y = -1250$ and $Y = -200$

camera 3 : measurements between $Y = -200$ and $Y = 0$

camera 2 and 1 : measurements between $Y = 0$ and $Y = 850$

4.3 Field measurements

4.3.1 DGPS-measurements

To be able to measure both the X,Y-coordinate and the Z-coordinate of the waterline a DGPS-system was used. One of the GPS-signal receivers was used as a reference point, located on the roof of a building high above the beach. The other receiver was placed on the front of a 4-wheel drive landcruiser. This GPS-system with reference station provides at least centimeter accuracy in X,Y and Z-direction.



Figure 4.2 DGPS-measurements of the waterline

During the daylight hours of 29th and 30th of November 1999, a total of 27 waterline datasets have been collected by driving along the waterline within 2 km of beach, between kilometer transect 38.750 and 36.750. Taking into account the Argus data collection schedule, which means always driving at the same location as the area filmed by the Argus cameras, it takes half an hour to collect one dataset. While driving, every 3 meter a measurement was done resulting in more than 16000 datapoints, each giving the X,Y and Z-coordinate of its location.

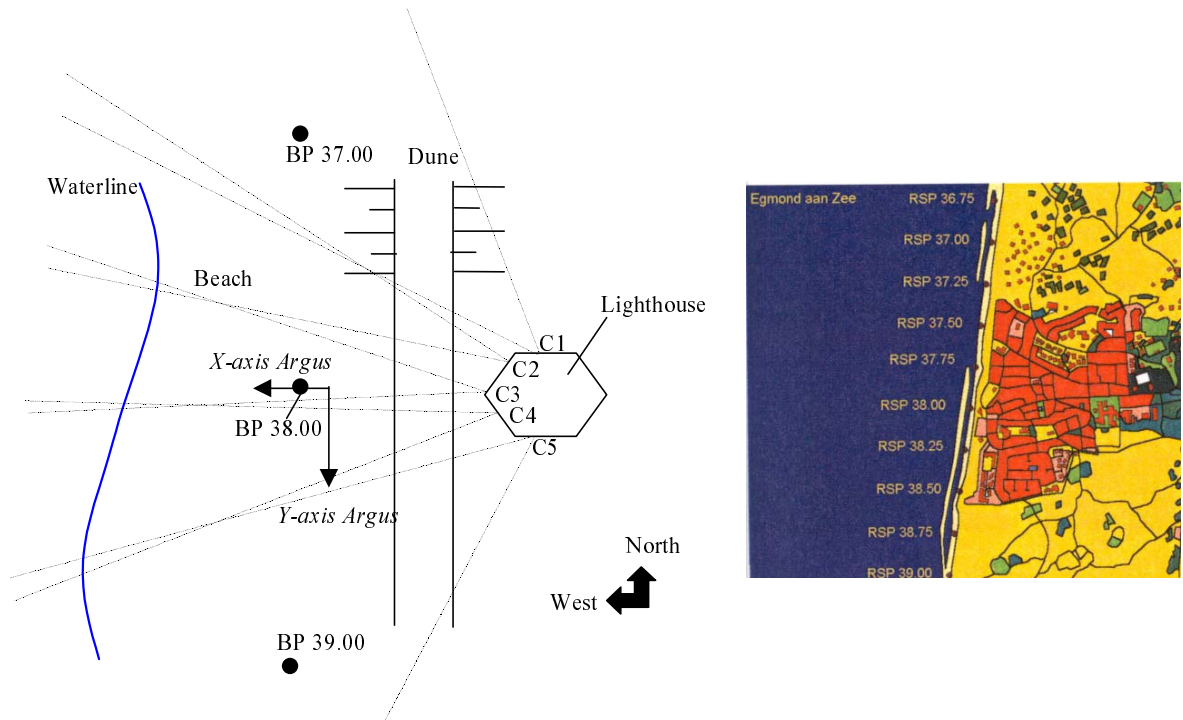


Figure 4.3 Kilometer transects at Egmond aan Zee, location of the lighthouse, the local coordinate system and a schematic sketch of the field of view of all cameras on the beach

The same approach has been used during the second field campaign, at the 14th and 15th of March 2000. For two days, during daylight hours, the waterline has been surveyed by a DGPS system with one of the receivers attached to a land cruiser. Rainy weather circumstances caused most of the first day images to be useless for model application (raindrops on the Argus lenses). The 15th conditions were good, especially during high tides the waterline was easy to detect.

Beside this a total intertidal beach profile has been surveyed between transect 37.00 and 39.00 longshore and in cross-shore direction from the dunes to the low waterline.

4.3.2 Swash-measurements

During the first field campaign a total of five video8 recordings of the swash zone were made. For determination of the location of the swash, a (cross shore) row of up to 10 stakes were placed in front of the camera in the swash zone. The most seaward stake (stake 9 in figure 4.4) was placed in the always wet area and the most landward stake (stake 1) in the always dry area. In this way the cross shore transect of stakes covered the whole swash zone. The GPS was used to determine their exact positions.

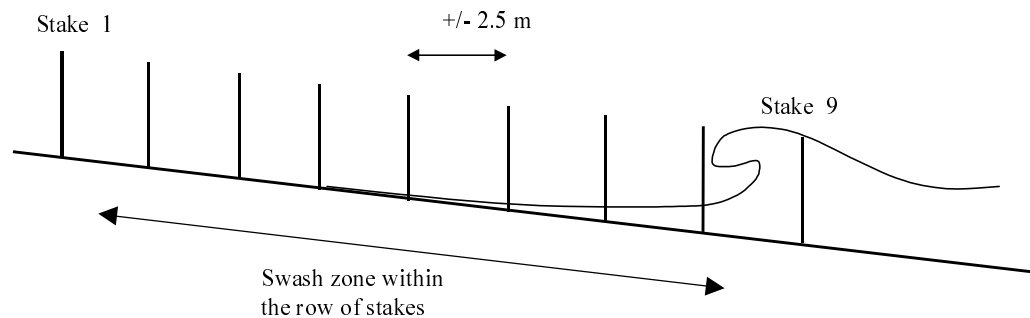


Figure 4.4 Row of stakes in the swash zone for finding the swash zone statistics

Because the positions of the stakes are known it is now possible to quantify the wave runup and rundown along this transect by using a digitisation technique, developed at the Department of Physical Geography, Utrecht University. This technique makes it possible to follow the waterline on a computer monitor with the mouse cursor, every 0.5 seconds the computer determines the location of the cursor and therefore the location of the waterline by using the coordinates of the stakes. The run-up time series obtained this way are used to make histograms of occurrence frequencies and exceeding curves. See the example in figure 4.5.

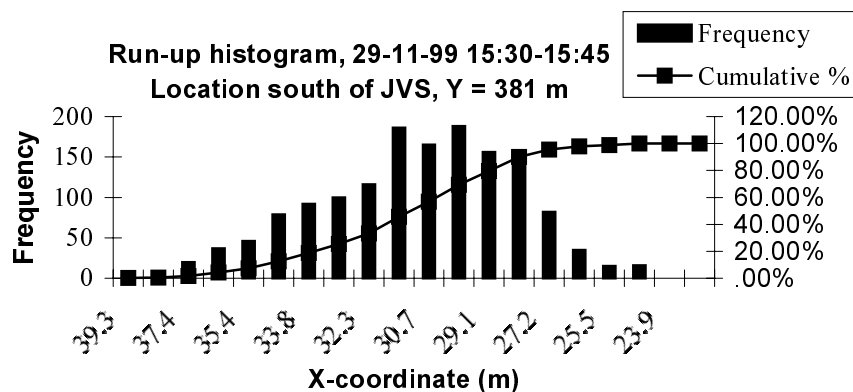


Figure 4.5 Run-up statistics as a result of a video recording of the swash zone

In this figure the swash zone is located between $X_1 = 23,9$ m and $X_2 = 39.3$ m, where X_1 is the most landward point of the swash zone and X_2 the most seaward.

Each recording took about 10 to 15 minutes and was synchronised with the accompanying 10 minute averaged Argus image. Recordings were made in the morning and the afternoon at different locations on the beach (see appendix D.1).

During the second campaign a total of five extra video recordings of the swash zone were made. Unfortunately these recordings are not worked out by the digitalisation technique. Manually, in front of a tv screen, it was possible to determine the location (x-coordinates) of the minimum and maximum runup along the transect of stakes.

4.3.3 Additional observations

The first campaign, at the 29th of November, the measurements started in the morning, approximately one hour after high tide. Waterlevels were several decimetres above NAP and because waves of considerable height could pass the shallowest breaker bar, the swash was eminent. The waterline ('glistening line') was easy to detect and to follow.

As the tidal level dropped, at most locations the waterline moved seaward with it. Except for some locations (especially near camera 4, between $\pm y = 200$ and $y = 500$) where the beach stayed wet even when the swash did not reach it. At those locations it was uncertain which 'line' to measure.

The most shoreward breaker bar became visible at tidal levels near NAP. Because of the channels through the bar, they look like small islands. At the shore side of these islands the waterline becomes more or less fixed, except for a few waves washing over the bar and inducing some swash. Although the breaker bar has his own seaward waterline, this line has not been measured. During the lowest values of the tide ($\pm \text{NAP} - 60 \text{ cm}$) the second breaker bar became visible.

The second campaign, during lower tides, the same kind of problems occurred again. Between approximately $X = 200$ to 500 m and around $X = -600$ some relative high areas on the intertidal beach stayed wet at lower tides. These areas could be up to about 15 cm higher as the waterline at other places, and were not influenced by swash.

Because the waterlevel above the inner bar decreased at lower tides the width of the swash zone decreased with it. This process went on until the bar got exposed and the waterline got fixed. Only the locations where rip currents flow through the inner bar still showed considerable swash.

So the biggest problem when measuring (and modelling, see section 3.2.4) the correct X,Y- and matching Z-coordinates is at the locations where the presence of wet areas indicate a swash zone which is not actually there. Another effect is the exposure of breaker bars at low tides causing multiple waterlines, when this happens it is not clear which line to measure.

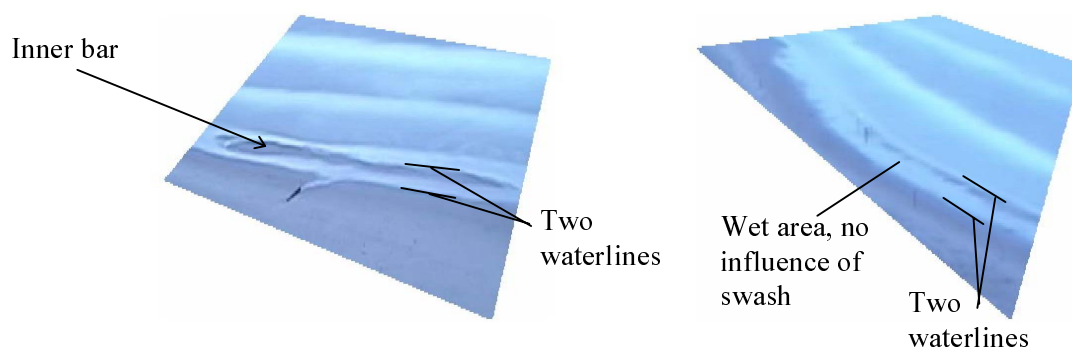


Figure 4.6 Argus images (regions of interest) indicating bar exposure (left) and wet areas on the beach (right)

4.4 Results and conclusions of the measurements

4.4.1 Waterline measurements

An example of the waterline measurements of one of the campaign days is shown in appendix E. It shows the horizontal (X,Y) and vertical (Y,Z) waterline as it has been driven for 30 minutes within the field of view of the cameras.

Obviously the horizontal waterline shifts seaward with dropping tide. The cross-shore intertidal range varies between 20 and 50 meters depending on the longshore location. The waterline beach levels vary between NAP -0.2 and NAP + 0.9, depending on the hydrodynamic conditions at the time.

Both, the March and the November dataset are satisfactory large and cover the whole intertidal beach area. Despite that, the problems about the wet areas and bar exposure made it hard to measure the waterline at lower tides. In section 4.3.3 it has been shown that the same conditions cause modelling problems. To avoid modelling problems and to maintain one unambiguous waterline it is therefore decided to use the waterline detection model for only relative high and medium tidal levels (tidal levels $> \text{NAP} - 0.2 \text{ m}$). Only for those circumstances one unambiguous waterline can be identified which also represents the location of the swash zone.

For model validation all of the waterlines that obey this criterion must be compared with model results. Nevertheless before validating it is important to take a closer look at the variation in the measurements themselves. For the horizontal X,Y coordinates this is hard to determine because of the strong long- and cross-shore variation in beach level. In the vertical direction this is easier as we aim to survey a (nearly) constant beach elevation. An example of a waterline measurement in the Y-Z space is given below.

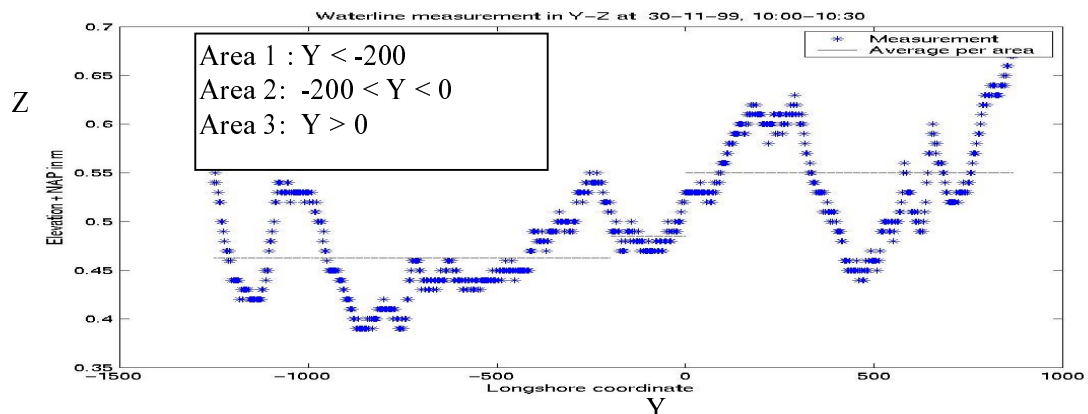


Figure 4.7 Waterline measurement in Y-Z

For determination of the error in the measurements, the longshore area is divided into three parts. These parts correspond with the areas filmed by the Argus cameras at ten minutes intervals. If the wave conditions and tidal level are assumed to be the same within an interval, the measurement should theoretically be horizontal. The figure shows this is not the case. To get an idea of the error in the measurements the following calculations have been made:

First the measured dots are interpolated to a grid which allows a measurement every 2 meter longshore. The average elevation per area Z_{average} is determined (horizontal lines in

figure 4.7). Next a calculation is made of the deviation between each interpolated dot Z_{measured} and its accompanying average:

$$\text{For each 2 meter longshore: } \Delta Z = Z_{\text{measured}} - Z_{\text{average}} \quad (4.1)$$

Thus, the distance ‘ ΔZ ’ indicates the deviation from the average for a certain measurement at a certain location.

This procedure has been carried out for all measured waterlines which are not influenced by the wet area and bar exposure problemacy. These are 10 cases for the November campaign and 17 cases for the March campaign. It results in 27 values of ΔZ at every 2 meter longshore between $Y = -800$ and $Y = 800$.

The root mean square value is calculated by:

$$\text{rms-value} = \sqrt{\frac{\sum_{n=1}^{n=27} (\Delta Z_n)^2}{n}} \quad (4.2)$$

Figure 4.8a shows the root mean square value of the ΔZ ’s at every 2 meter long shore. Figure 4.8b shows the averages and standard deviations of the ΔZ ’s at every two meter longshore.

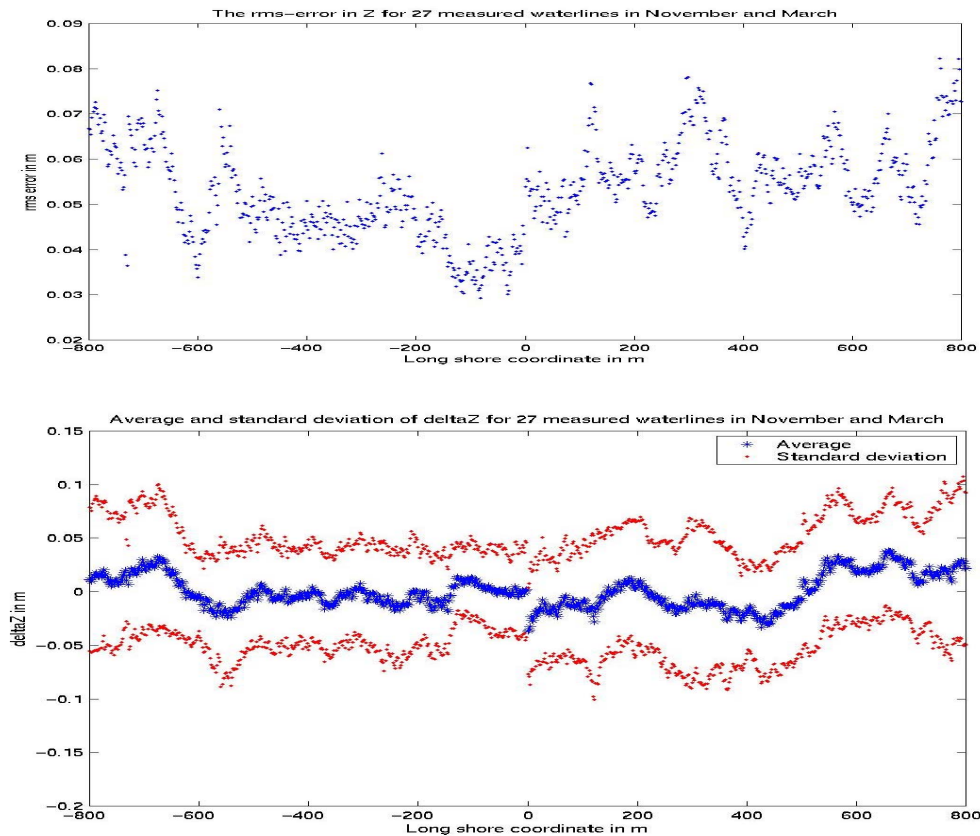


Figure 4.8 The rms-value of the variation in the measurement itself every two meter longshore (above) and the average value and standard deviation of ΔZ every two meter longshore (below)

The rms values vary between 0.03 and 0.08 m which is of the same order as the standard deviation around the average. On a beach slope 1:40 such errors mean only a few meters in cross shore direction. Taking into account the fact that all measurements have been done by driving a car on a irregular beach along an arbitrary line, these kind of variations are logical and acceptable. For validation however these variations must be kept in mind.

4.4.2 Video recordings of the swash zone

The statistic results from the swash video recordings of November are shown in appendix D.1. From the diagram, the location of 5% respectively 95% swash exceedence can be determined. Besides, every swash video has been recorded at a beach location that corresponds with a time averaged Argus image. This means the car, measuring the waterline, also crossed the swash video transect while recording. The results are given in appendix D.2. for each swash video together with the waterline measured by the GPS and if possible, the accompanying model results. Table 4.1 shows the relevant information for each video of the November campaign.

Date	Time (GMT)	Location (m)	Tidal level (m +NAP)	Hrms (m)	minX 5% (m)	maxX 5% (m)	Swash length (m)
29/11/1999	11:15-11:30	Y = -651	0.45	1.17	xxx	xxx	xxx
29/11/1999	14:30-14:45	Y = 381	-0.40	0.86	27	36	14.0
29/11/1999	15:00-15:10	Y = 381	-0.42	0.79	28	36	11.9
30/11/1999	08:27-08:42	Y = 557	0.47	0.88	8	24	+/- 20
30/11/1999	10:10-10:22	y = -39	0.07	1.05	75	89	19.2

Table 4.1

The swash videos from the March campaign have not been digitised. Only the locations of minimum and maximum swash could be estimated from the videos. These locations were estimated somewhere near 5% and 95% exceedence. The error made by just estimating the location from the screen will only be about half the length between two stakes. This means 1 to 1.5 m. The results are shown like the November case in appendix D.2. All relevant video information can be found in table 4.2.

Date	Time	Location (m)	Tidal level (m)	Hrms (m)	minX (m)	maxX (m)	Swash length (m)
14/3/2000	08:00-08:10	Y = 201	0.76	0.63	-6.21	7.64	13.85
14/3/2000	09:00-09:10	Y = 201	0.93	0.62	xxx	-8.79	xxx
15/3/2000	09:45-09:55	Y = -366	0.65	1.65	33.44	52.01	18.57
15/3/2000	10:20-10:30	Y = -366	0.74	1.59	33.60	51.10	17.50
15/3/2000	11:30-11:40	Y = 475	0.65	1.41	-21.97	-8.82	13.15

Table 4.2

For all cases where a model solution can be determined (1 November video and 4 March videos) the waterline modelled by the waterline detection technique corresponds remarkably well to the measured waterline. For the time being it is concluded the chosen 'glistering line' is the waterline found by the waterline detection technique. The error band for this waterline is the error found in the measurements.

Furthermore it is important to know where this line (= the waterline) is located within the swash zone. The dot which marks the cross shore position at where only 5 % of the run-up

passes is for most cases located around this line. This corresponds also to the authors own experience in the field. Still some of the results show differently, the 5 % exceedence position can be either landward (e.g. video 29-11-99, 11:15-11:30) or seaward (e.g. video 30-11-99, 10:10-10:22). These differences are only a few meters, which can easily be the avoiding route of the car when passing the stakes. Consequently it is decided that the model finds the waterline at the outer edge of the swash zone, at a location where only 5 % of the swash passes.

The last remark concerns the fact that the observations in the field show a diminishing swash length as the tidal level drops. The waterline eventually gets fixed at the lowest tides when the inner bar eliminates swash and surfbeat. The swash video results indicate the same thing. This proves the approach that swash heights are reduced by decreasing waterdepth above the inner bar. The swash is totally blocked when the inner bar is exposed. Only a few beach locations directly in front of rip currents still showed some swash, there the waves are able to penetrate through the rips. Such locations could cause errors when modelling the Z-coordinate.

4.4.3 Summarising the results

On the basis of the results from the field measurements, the following conclusions have been made:

1. For the Argus site 'Jan van Speijk' the waterline detection technique can only successfully be used for tidal levels approximately above NAP -0.2 m.
2. The rms-error for the waterline measurements ranges between 3 and 8 cm in vertical sense.
3. The measured waterline corresponds to the modelled waterline.
4. This waterline is located at the cross-shore location where only 5% of the wave runoff passes.

Knowing these conclusions the waterline detection model can be validated.

4.5 Model validation

The waterline detection model consists of two methods: Argus modelling of the horizontal waterline coordinates and hydrodynamic modelling of the associated elevation. Both techniques can be validated by comparing the model results to waterline measurements. Consequently, the validation can be carried out in three directions: in X (cross-shore), in Y (longshore) and in Z (height). Still it is important to keep in mind that any errors in X ($=\Delta X$) and Y ($=\Delta Y$) also cause an error in Z ($=\Delta Z$) and vice versa.

This is why the error in all three directions is expressed as an error in Z.

This means:

- the error in Z caused by an error in X, $\Delta Z_x = m_1 \cdot \Delta X$
 - the error in Z caused by an error in Y, $\Delta Z_y = m_2 \cdot \Delta Y$
 - the error in Z caused by an error in Z, $\Delta Z_z = \Delta Z$
- m_1 is the beach slope in cross-shore direction, m_2 the longshore beach slope.

When assuming $m_2 \ll m_1$ the contribution of ΔZ_y to the total error in Z can be neglected. Consequently the total error in Z can be written as:

$$\Delta Z_{tot} = \Delta Z_x + \Delta Z_z \quad (4.3)$$

The following figures explain this approach. Figure 4.9a shows the situation when the model predicts the height correct but the horizontal location is too far seaward. The error ΔX can be translated into an error ΔZ_x at the horizontal model location. Figure 4.9b shows a perfect X but the model calculated the height too high. The error ΔZ_z is simply the difference in Z between model and measurements.

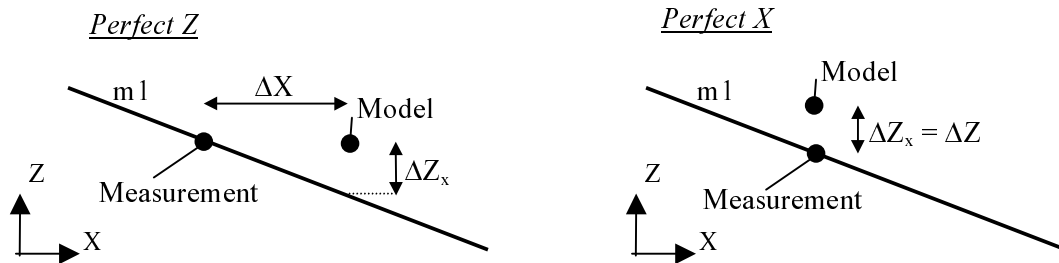


Figure 4.9 Differences between model and measurement in X and Z both expressed as an error in Z.

But neither X and Z are perfect. The modelled X can be either landward or seaward of the measurement, the modelled Z can be either higher or lower than the measured Z. This means both errors ΔZ_x and ΔZ_z can either compensate each other for the total error or amplify the total error depending on the location of the modelled waterline. This is explained by figure 4.10

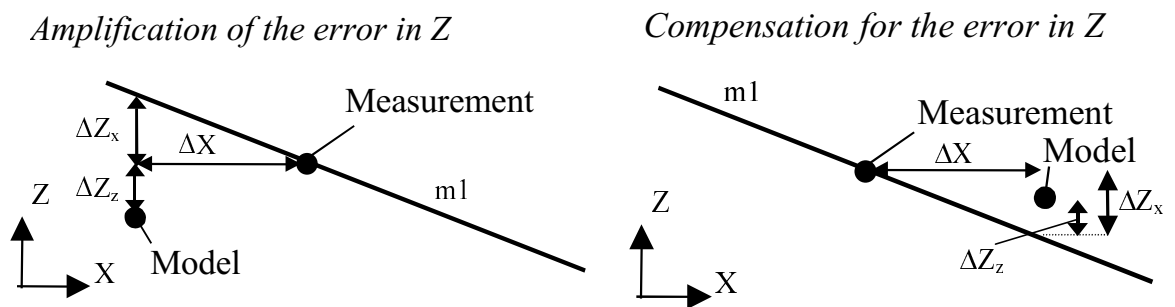


Figure 4.10 Amplification and compensation for the error in Z

In this section the error in X will first be treated to find the accuracy of the waterline detection technique. Next, the error in Z to find the accuracy of hydrodynamic modelling of the waterline height. Finally the accuracy of the whole waterline detection model will be determined.

4.5.1 Validation waterline detection technique

Each modelled waterline part consists of a certain amount of non-uniformly spaced X,Y-coordinates. These coordinates are treated with a 1D-interpolation method which structures them until there is a waterline coordinate every 2 meter in Y-direction. The same procedure is carried out for the measured coordinates. This means that within the areas where both lines exist, the cross shore difference ΔX between model and measurement can be identified every two meter in Y (long shore).

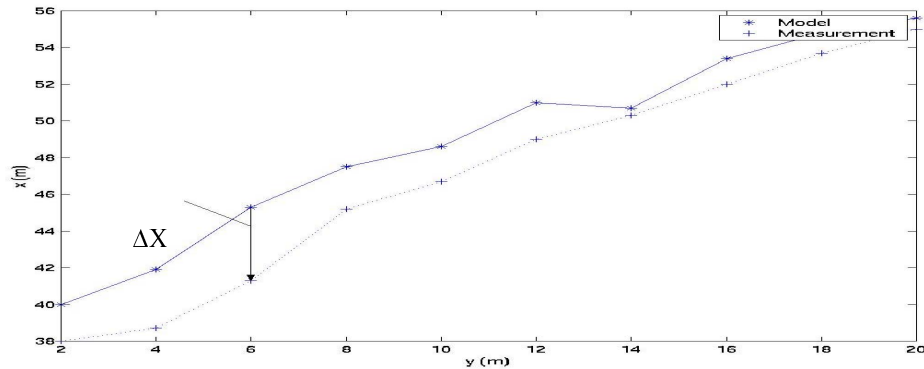


Figure 4.11 Measurements and model results interpolated to a grid

This procedure has been carried out for all dates and times at which model results in combination with measurements exist. It resulted in maximal 16 values of ΔX per 2 meter longshore.

Next, all values of ΔX are multiplied by the cross-shore slope m_1 to get just as many values for ΔZ_x . Based on the results from the measurements a value of 0.025 was taken for m_1 .

The root mean square values of ΔZ_x are shown in figure 4.12 for all longshore locations with more than 5 values of ΔZ_x . In a formula this reads:

$$\text{For every two meters in Y: } rms - error = \sqrt{\frac{\sum_{n=1}^{n>5} (\Delta Z_{xn})^2}{n}} \quad (4.4)$$

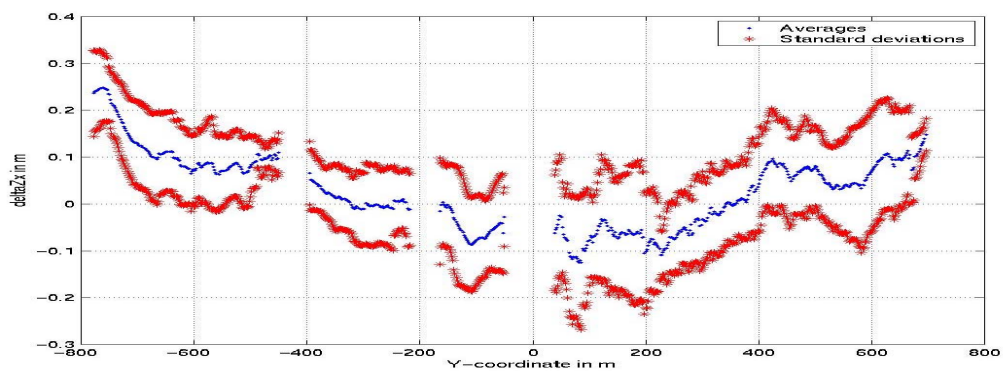
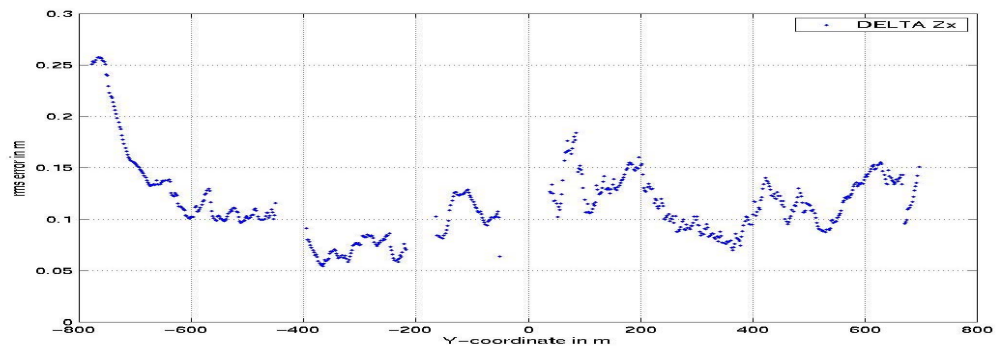


Figure 4.12 The rms-error in Z caused by cross-shore differences between model and measurements (above) and the average values and standard deviations of ΔZ_x

The figures shows that deviations between model and measurement in cross-shore direction cause root mean square errors in Z typically in the order of 10 to 15 cm. Also the standard deviation shows these kind of errors. These kind of errors are intra swash and acceptably small.

Only for locations < -700 m the errors increase fast. First guess would be that it is caused by the increase in pixel resolution at larger distance from the camera (Fig. 2.3). Because of this, the waterline detection technique will find a smaller amount of waterline pixels at larger distances from the camera. This might cause bigger errors when determining the waterline in fieldcoordinates (section 3.2.3).

A closer look at the model results indicates that this might not be the only reason. The relative extensive field of view of the outer cameras shows, apart from the wet-dry areas, also color differences in longshore direction. Especially due to difference in light and dark. Some of the dry pixels at the far end of the image are therefore considered wet (figure 4.13).

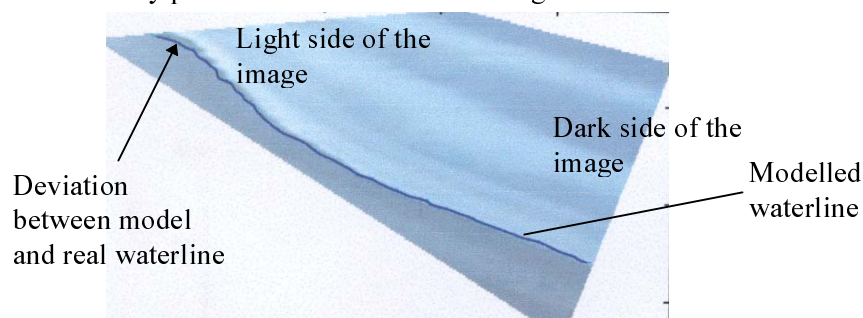


Figure 4.13 Long shore color differences

The problem can be solved by considering more than one region of interest inside an Argus image. This reduces the longshore color differences and helps the technique to discriminate better between dry and wet (see also chapter 6, conclusions and recommendations). This means the waterline detection model has to be modified. These modifications can be something to work on in future work. For the continuation of this study the errors are accepted.

4.5.2 Validation of the waterline height

Basically the same approach as for the error in X has been used to determine the error for modelling the waterline height. Figure 4.14 shows an example of model results in combination with measurements for one case. Because the tidal dataset provides a new value every 10 minutes, the model is able to calculate three waterline heights within 30 minutes of measurements (straight lines).

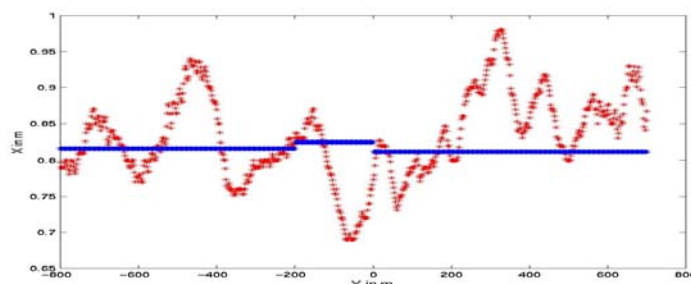


Figure 4.14 Elevation of the waterline, measurements (dotted) and modelled values (straight lines)

First the measured dots and the modelled lines are interpolated to a grid which allows values of Z every two meter longshore. The differences between model and measurement can be determined. It results in up to 27 values of ΔZ per two meter longshore. The root mean square values are plotted in figure 4.15.

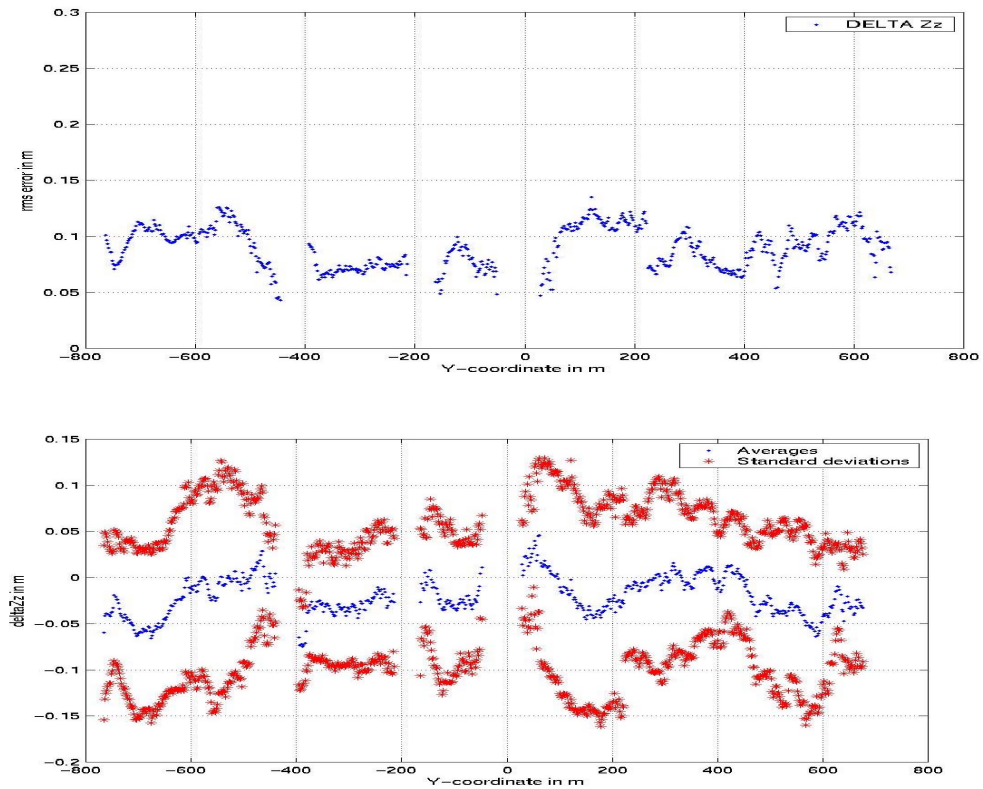


Figure 4.15 The rms-error in Z caused by differences in waterline height between model and measurements (above) and the average values and standard deviations of ΔZ_z

These results show the rms errors and standard deviations amounting only about 10 cm, very near the errors in the measurements itself (3 to 8 cm). This proves that hydrodynamic modelling of the waterline is quite accurate.

4.5.3 Validation of the whole model

To translate the above results to a total rms error of the model, the values of ΔZ_x and the accompanying ΔZ_z have been added with the correct sign for the direction. This means sometimes the error increases and sometimes the errors compensate for each other. This resulted in up to 16 values of ΔZ_{tot} every 2 meter in Y .

The result is figure 4.15, after calculation of the rms-error for all values of ΔZ_{tot} every two meter longshore between $Y = -800$ m and $Y = 800$ m.

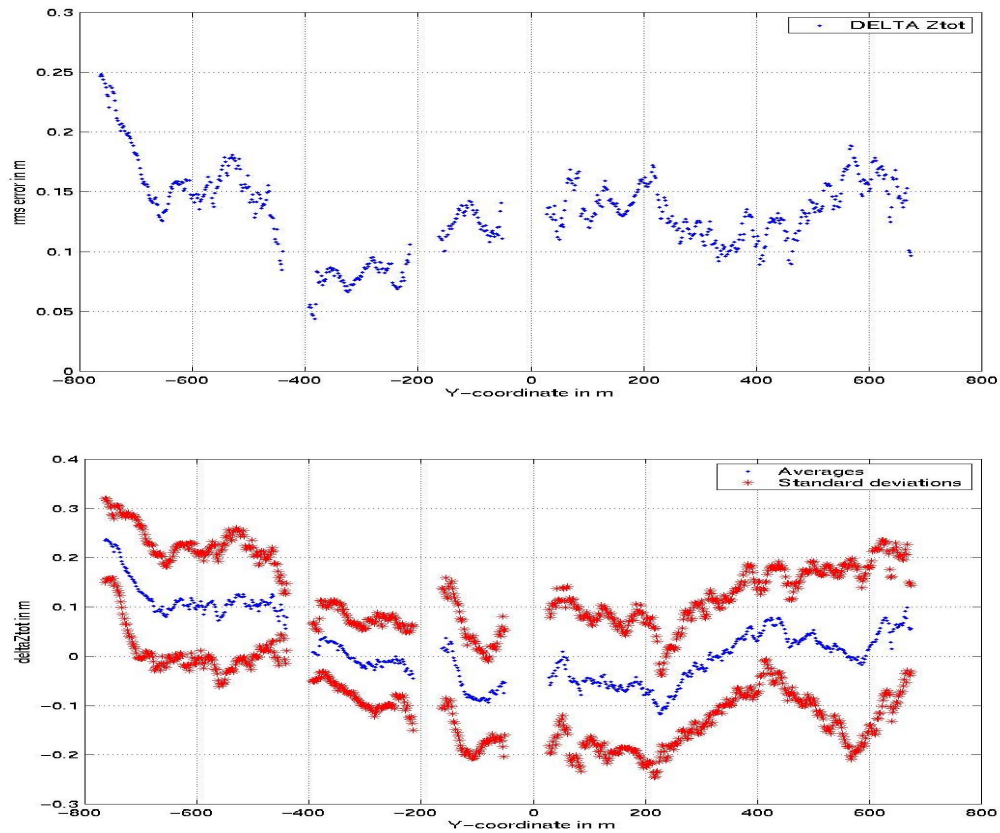


Figure 4.16 The total rms-error in Z due to differences between model and measurements in height and cross-shore distance (above) and the average values and standard deviations of ΔZ_{tot} .

Except for the location $Y < -700$ all rms errors are located between 0.05 and 0.2 m. In a horizontal sense on a slope 1:40 this means 2 to 8 meters. These kind of errors seem very acceptable considering other influences like:

- The pixelresolution: errors between 0 and 1m cross-shore and 0 to 8 meter longshore.
- Variation in the measurements: horizontal variation from 1.2 to 3.2 m
- Waterlevel changes within 10 minute intervals: cross-shore errors from 0 to 6 m.
- Errors brought in by averaging over the width of the swash zone when using the waterline detection technique, order 10 m cross-shore.
- Errors brought in by using empirical formulas and estimations for modelling Z: unknown

In conclusion, knowing the models accuracy the waterline detection model is a powerful tool for determination of waterline locations within the intertidal beach. With the help of this model intertidal beach profiles can be created, which is described in chapter 6.

5 Evaluation of the Egmond beach- and shoreface nourishments between June 1999 and June 2000

5.1 Introduction

In order to get insight in the coastal morphology at Egmond aan Zee we make use of the available Argus tools. In this chapter the automatic tools to generate merged- and stacked images in combination with the waterline detection model are used to determine the morphological changes of the beach and sand bars at Egmond between June 1999 and June 2000. Finally this provides enough information to allow a qualitative and quantitative evaluation of the effect and behaviour of the beach- and shoreface nourishments during this period.

Before doing so a more general description is given about beach- and shoreface nourishments and the expected effect of such a combination of nourishing. This will be useful in order to understand and describe the Argus observed morphologic changes.

5.2 Sand nourishments

5.2.1 Nourishing in general

A sand nourishment takes place to artificially increase the amount of sand in a coastal area with sand originating from outside that area.

The type of nourishment can be characterised by its location in the profile. In cross-shore direction three types can be distinguished (TAW, Basisrapport zandige kust, 1995):

- dune nourishment
- beach nourishments
- shoreface nourishment

In contrast with dune nourishments, beach- and shoreface nourishments are most of the time under the influence of waves, wind and tide. In time these nourishments will deform due to the working of sediment transport.

In case of structural erosion, loss of sand can be compensated by periodic nourishing. In this way it is expected that the minimal location of the coastline can be maintained for a certain period of time. Thus, sand nourishments in an eroding coastal area must be repeated. The expected lifespan and repeating time is mainly determined on the basis of profile measurements.

5.2.2 Beach nourishments in general

When carrying out a beach nourishment the volume of sand in a coastal area is enlarged by a direct expansion of the beach volume (TAW, Basisrapport zandige kust, 1995).

In time a beach nourishment deforms under the influence of sediment transport with a rate depending on the hydrodynamic conditions and the sediment characteristics. In general larger transport rates occur for smaller grain sizes.

In cross-shore direction the volume of sand will redistribute by cross-shore transport processes. The eventual shape of the nourishment (slope, spreading in seaward direction) will fit with the local average hydrodynamic conditions and grain size. Redistribution in cross-shore direction might also cause sand loss.

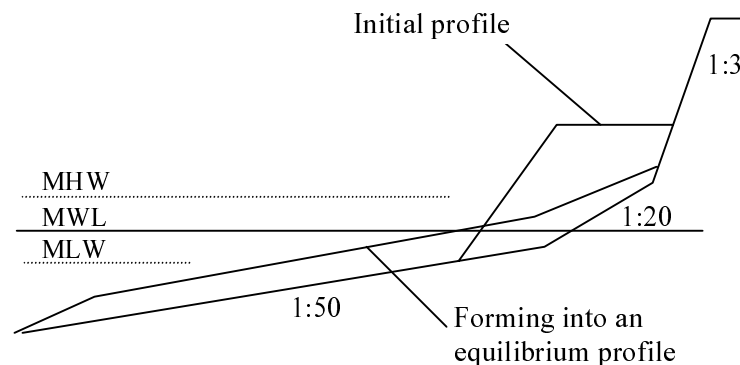


Figure 5.1 Deformation of a beach nourishment in cross-shore direction under the influence of waves and tide

The influence of longshore transport processes will also deform a beach nourishment in longshore direction. Sand that disappears this way will directly be transported to the neighbouring coastal area.

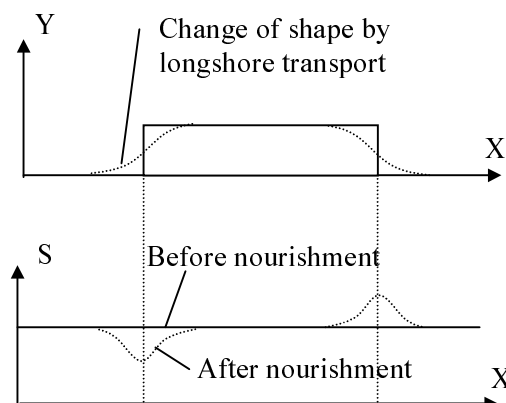


Figure 5.2 Deformation of a beach nourishment in longshore direction by longshore sediment transport

The influence on the morphological system by a beach nourishment is not that clear. In general it is accepted that, unless there are big differences in sediment characteristics, there will be no significant influence on the morphological system. If a beach nourishment does have influence on the morphological system it results in a change of the trend in the development of the amount of sand. Consequently, it results in a change of the trend in development of the coast.

So, the execution of a beach nourishment will have a clear effect on the location of the coastline. The effect it has on the development of the coast will generally not be that big.

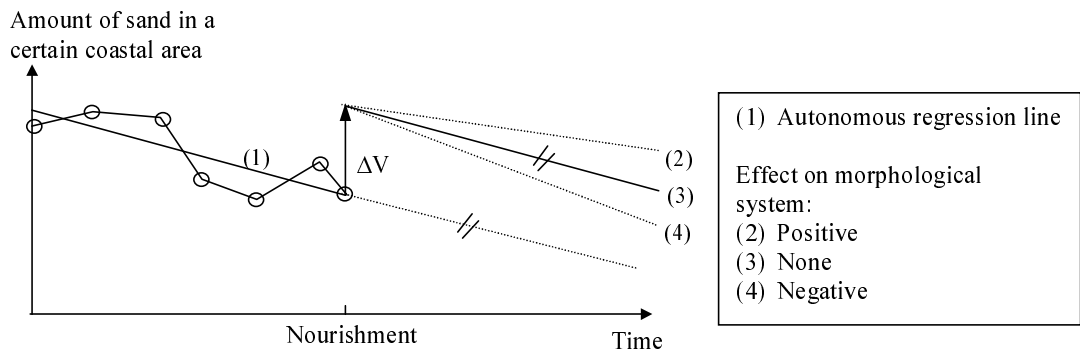


Figure 5.3 Possible effects of a (beach) nourishment on the morphology

When a beach nourishment on an eroding coast has been carried out, two situations can occur:

- The shoreface erodes, for example because of a gradient in tidal driven long shore transport. Gradual beach erosion will occur due to longshore transport on the shoreface. The occurring cross-shore transport processes (redistribution) cause the beach to act as a sediment source for the loss of sand on the shoreface.
- Erosion of the beach, primary caused by transport processes near the beach itself. For example because of a gradient in wave driven longshore transport in the breaker zone.

The second situation will probably cause a more gradual decline of the added volume of sand than the first situation. In the first situation cross-shore transport is an essential link in a series of processes. A long unbroken calm period will for example be able to stagnate the outflow of nourished sand in seaward direction.

5.2.3 Beach nourishment in combination with a shoreface nourishment at Egmond

The behaviour and the effect of a combination of beach- and shoreface nourishments is still not clear. Nevertheless, it is decided that it is a good alternative for solving the Egmond coastal problemacy. It is expected that a shoreface nourishment will have a positive influence on the following aspects (Boers, 2000):

- Extension of the neighbouring coastal areas
- Interruption of longshore transport
- Providing sand for the BCL-zone
- Protection of the BCL-zone

These four aspect are described below:

- Extension of neighbouring coastal areas

A shoreface nourishment means a lower cost price per cubic meter of nourished sand. This means, in comparison to a beach nourishment, a larger amount of sand can be placed. Consequently a larger amount of sand is available for neighbouring coastal areas. If the sand is transported to the neighbouring areas it means the areas next to the boulevard (no buildings) should show coastal progress and extension. The location of the coastline at Egmond will therefore not stick out too much with respect to the neighbouring coastal

areas. It is expected that a number of such nourishments eventually increases the life span of these nourishments.

- Interruption of longshore transport ('breaker berm')

Due to the wave dimming effect of the shoreface nourishment, the wave driven longshore transport will decrease landward of the nourishment. As a result the tendency for erosion will decrease. Still it is important to realise that cutting of the longshore transport might induce erosion at neighbouring areas (at the lee side of the nourishment).

- Providing sand for the BCL zone ('feeder berm')

Asymmetric incoming waves may cause cross shore transport towards the coast. As a result, nourished sand might end up within the BCL zone. This means the shoreface nourishments 'feeds' the beach with sand.

Besides this, rip currents can occur. These circulating currents might have an extra effect on cross shore transport towards the coast.

- Protection of the BCL zone

The wave dimming effect of the shoreface nourishment might have another positive effect on the combination of a beach- and a shoreface nourishment. Because a large part of the incoming wave energy dissipates by breaking over the shoreface nourishment, the rate of redistribution of sand in cross-shore direction will be less. The beach nourishment will therefore exist longer. Thus, a reduction of off-shore losses due to cross-shore transport.

Besides this, the wave dimming effect might change the location pattern of existing rip currents. Until now the consequences of this effect are not known.

5.3 Intertidal beach morphology

The previous sections described the possible effects when applying a beach- and a shoreface nourishment. Clearly, nourishment behaviour like that must be noticeable on the beach at Egmond. The waterline detection model has been used to study this.

With the help of the waterline detection model it is possible to collect waterlines within the intertidal beach. By modelling multiple waterlines from Argus images within one or two successive tidal cycles it is possible to create an intertidal beach profile for that time. A series of profiles in time will determine the effects both nourishments have on the Egmond beach.

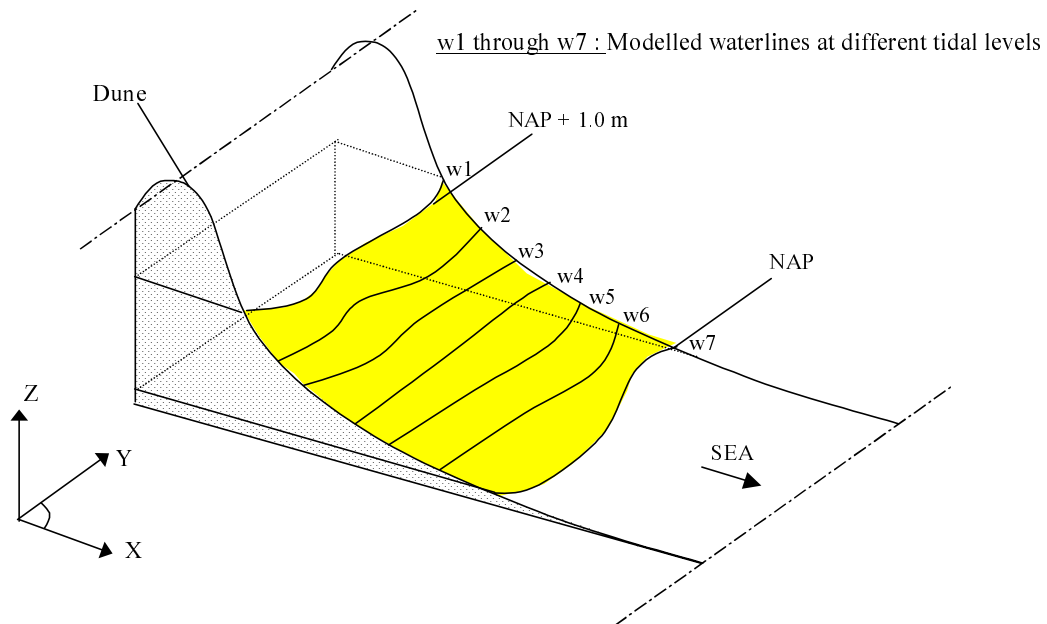


Figure 5.4 Intertidal beach profile build out of multiple modelled waterlines

To start modelling waterlines it is at first important to choose a 'suitable' day or series of days with respect to the quality of the images. This avoids most modelling problems and consequently allows a bigger amount of solutions.

When enough waterlines have been modelled and collected, sufficiently spread along the intertidal area, the X,Y and Z coordinates of all waterlines are put into an automatic routine for creating the intertidal beach profile.

This working of this routine is described below:

First all coordinates are interpolated to a grid. In longshore direction between $Y = -700$ m and $Y = 700$ m, the spatial step amounts 5 m. In cross-shore direction between $X = -40$ m and $X = 120$ m, the spatial step amounts 1m.

Next is cutting of the edges based on height. All calculated datapoints above $Z = \text{NAP} + 1,0$ m are assumed to be at 1,0 m NAP. All datapoints below NAP 0 m are assumed to be at NAP 0.

The reason for doing so lays in the fact that only between those values of Z enough model solutions can be found. The applicability of the waterline detection model defines the lower boundary (see section 4.4.3) while the tidal elevation defines the upper boundary (MHW = NAP +1.0).

The result is shown in figure 5.5, where the intertidal beach has been determined based on waterline detection from Argus images recorded at the 5th and the 6th of June.

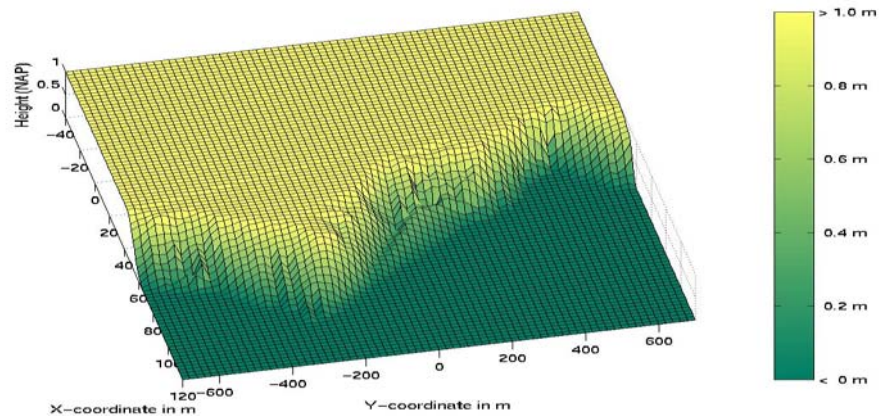


Figure 5.5 Modelled intertidal beach profile for June 1999

Based on the first year of Argus images from Egmond site ‘Jan van Speijk’ the waterline detection model has been used for the determination of these bathymetries. For each month between June 1999 and June 2000 one or two ‘suitable’ days have been selected and the intertidal beach profile has been determined. The results are shown in Appendix F.1, the 3D profiles are plotted as a planview, the contour lines indicate the height within the intertidal area.

The first interesting observation that follows from these results is the very irregular shape of the coast. All pictures show the coast sticks forward around $Y = -200$ m whereas a gap appears near $Y = 400$. Later it will be shown that this gap is caused by a rip current.

The beach nourishment in April 1999 has been carried out over 1.5 km, between kilometre transect 37.25 and 38.75. This corresponds to the area between longshore Argus coordinates -750 m and 750 m.

Generally seen the first four months, from June 1999 to September 1999, the location of the intertidal beach stays the same. The relatively calm meteorological conditions during these months cause no erosion but also show no significant extension of the coast.

In October the stormy season sets in, the intertidal beach retreats at all longshore locations. This goes on in November, it shows that within two months the coastal retreat is up to 30 meters.

After this period the erosion seems to hold at most locations, except for the area between $Y = -400$ and $Y = -600$. A second ‘gap’ is created which leaves a very irregular coast with a tongue of land stretching out near $Y = -200$ m (January, 2000).

In February and March the rip near $Y = 400$ m starts to continue going landward. During the field campaign in March it was clearly visible that at this location the intertidal beach reached the dunes. The erosion scarps at the dune foot indicated dune erosion.

The intertidal beach profile of April shows the beginning of a calmer period and consequently the beginning of beach recovery. At all locations the intertidal beach builds up especially between $Y = -200$ and $Y = -400$. Here the intertidal beach recovers extremely

fast, the one meter contour stretches out beyond the location it had during the summer of 1999.

May shows the intertidal beach at both rip locations builds up. The intertidal beach profile between $Y = 0$ and $Y = -400$ is harder to determine. The reason for that is a complex system of gully's and bars in front of camera 3. The beach profile is too irregular for finding the intertidal beach profile from waterlines. This is explained by the following Argus images:



Figure 5.6 Argus images from camera 3 at 15-04-2000(left) and 15-05-2000(right)

Figure 5.6 shows the beach at low tide between approximately $Y = -250$ m and $Y = 50$ m at the 15th of April and the 15th of May 2000. The tongue of land is clearly visible indicating a complex structure of gully's and bars. Consequently, it is hard to identify unambiguous waterlines at most tidal levels. It explains the blank area in the modelled intertidal beachprofile of May. The contours of the intertidal beach profile May near the blank area can therefore not considered to be very precise. Nevertheless it gives an indication of what is happening at that location, viz. extension of the beach.

Finally the intertidal beach profile of June shows the profile after one year of modelling. Most striking observation is the fact that the intertidal beach has retreated a bit compared to May whereas from the aspect of seasonal fluctuations it is expected to build up. It might be the result of an unexpected storm which occurred the 28th of May 2000. Still, compared to the intertidal beach profile of June 1999 the intertidal beach is shifted landward. Nevertheless, since the beach state of June 1999 was one of nourished state, this is not that strange. Clearly visible is the effect of cross-shore redistribution of sand. The relatively steep profile of June 1999 (2 months after the beach nourishment) is transformed into a more gradual profile.

5.4 Bar behaviour

The behaviour of sand bars has been studied with merged images. Appendix F.2 shows one image for each month between June 1999 and June 2000. The time and date of all images correspond with tidal levels near NAP -0.4, the conditions are preferably chosen for high waves (hence clear dissipation patterns).

The shoreface nourishment is located between longshore Argus coordinates -1100 m and 1100 m, at a cross-shore location near $X = 700$ m (it was placed in July/August 1999).

The first image from June 1999 shows a complex multiple bar system. Because the tidal level of all images is around NAP -0.4, the inner bar ('swash bar') is exposed. Behind the first bar (swash bar) a second (between $X = 80$ and $X = 175$), a third ($\pm X = 225$ m) and even a fourth breaker bar ($X = 500$ m) can be identified.

The beach nourishment is clearly visible, especially between $Y = 100$ and $Y = -900$. It looks like the centre point of the beach nourishment shifted north between April 1999 and June 1999. The second breaker bar bends around the beach nourishment and seems interrupted at $Y = -300$ m, the third and fourth bars stay reasonably straight. A rip current can be identified in the third breaker bar near $Y = 500$ m. This probably is the reason for coastal retreat at the same location on the beach (see the intertidal beach profile of June 1999).

The merged images of July, August and September show the same system of bars. Bar locations stay almost the same, although it looks like the third breaker bar gets more and more 'unstable' (it starts twining a bit and more rip currents appear). Furthermore there are no signs the beach nourishment moves more north. The shape of the nourishment is a bit asymmetric, the center point is located around $Y = -250$ m.

The first signs of the presence of the shoreface nourishment appears on the merged images of October. A dissipation pattern around $X = -700$ can be identified.

Going into November no striking morphological changes can be detected. Bar locations and the shape of the beach nourishment stay the same. The rip current at $Y = 500$ m seems to have disappeared, despite the fact that the intertidal beach profiles of October and November still show erosion at that location.

On the merged images of December some remarkable changes occur. The second and third breaker bar move seaward at the location of the beach nourishment. Both bars clearly bend around the centre of the nourishment at $Y = -250$ m. Unlike the other bars, the fourth breaker bar seems to move landward (a shift of approximately 50 to 75 m). The same system is visible on the merged images of January although it looks like the fourth breaker bar keeps on moving landward.

Still, the shoreface nourishment can be identified only vaguely.

A storm in February shows broad intensity patterns above all bars. Even the shoreface nourishment is clearly visible along $X = 700$ m. The second, third and fourth breaker bars stay close to each other near the centre of the nourishments. The distance between the third and the fourth bar amounts approximately 125 meters in front of the beach nourishment while it amounts about 300 meters to the sides. The angle between the bar and the longshore axis can be up to 30° .

March and April still show the same pattern. The locations of the bars stay the same, the centre of the beach nourishment tends to shift a bit south to $Y = -150$ m. The calmer conditions of April clearly show the extension of the beach at this location.

It also is interesting to follow the twist in location of the second and third breaker bar. The cross-shore variation in these bars amounts about 175 m (between the position at $Y = 450$ m and $Y = -150$ m).

A late unexpected storm arrived at the Dutch coast at the end of May. The bright intensity patterns show the shoreface nourishment moved a bit landward.

The last merged images of June show calmer circumstances. Bar locations stay the same and the extension of the beach, centred near $Y = -250$, m seems to be a bit shifted to the north.

In conclusion, the time series of merged images show a complex multiple bar system. During the stormy winter period the bars start moving. The shoreface nourishment and the fourth breaker bar near $X = 500$ move a bit landward. The other bars start curling around an extension of the beach, 250 m north of the original centre of both nourishments. It looks like the shoreface nourishment protects and/or feeds the beach at this location. Furthermore the location of beach erosion seems to correspond with the location of rip currents.

At two locations, for the extension of the coast at $Y = -250$ m and for the location of the rip at $Y = 600$, stacked images have been made at tidal levels around NAP -0.4 m. These images also show the movement of the breaker bars along the transect $Y = -250$ m and the relative stable position of the bars along $Y = 600$ m (see appendix F.3).

5.5 Beach width

The reason for applying a beach nourishment is, beside maintenance of the coastline position, to create enough beach width for recreation. Especially in the summer months it is important to have enough space between the dune foot and the high tide waterline.

The shoreface nourishment has been placed to protect the beach nourishment. It is meant to dissipate the highest waves and to act as a sand source for the beach. It is therefore expected to have a positive effect on beach width.

Besides it is hoped that both nourishments will have a life span of at least a few years.

The longshore area where sufficient beach width has to be maintained is considered to be the same as the nourished area, between $Y = -750$ m and $y = 750$ m in local Argus coordinates.

When taking a close look at Argus- and merged images beach pavilions can be identified on locations near $X = -25$ m just in front of the dunes. The pavilion and the beach area around it is in use for recreation (figure 5.7). It is desirable that this maintains a dry beach area as much as possible. So roughly the zone between the dune foot and the $X = 0$ line stays preferably dry.



Figure 5.7 Beach pavilion at Egmond

Based on the results from the time series of intertidal beach profiles and merged images it has been shown that between June 1999 and June 2000 the beach width constantly changes depending on the longshore location.

At most locations beach width is preserved, except for the area south of $Y = 200$. The intertidal beach profiles show a large erosion hole centred around $Y = 400$ and $Y = 500$ m. During the worst month (March), the intertidal beach reaches the dunes. So, within 11 months, between the placement of the beach nourishment in April 1999 and March 2000, no beach width is left at this location.

The beach between $Y = 0$ and $Y = 400$ shows the opposite effect. Some sort of tombolo effect is visible. At these locations the wave dimming effect of the shoreface nourishment cuts off longshore transport and the beach can extend.

North of this location the beach tends to do the same as in the south. Some merged images which are not shown in this report also indicated rip currents, centred near $Y = -750$ m.

In conclusion, during the considered period beach width is not preserved at all locations along the Egmond beach between $Y = -750$ m and $Y = 750$ m. Extension of the coast, probably due to the presence of the shoreface nourishment, occurs only locally. South of this extension, the beach(nourishment) seems more vulnerable. Large amounts of sand disappear at this location. An already visible trend of beach recovery in the more calm summer months of 2000 might have compensated the loss of sand at these locations. Still the authorities decided to nourish the area between $Y = 0$ and $Y = -1000$ m in July 2000.

6 Conclusions and recommendations

6.1 Introduction

The morphology of the Egmond coast between June 1999 and June 2000 has been determined with the help of several Argus video-based tools. Time series of intertidal beach profiles and merged images have successfully been used for evaluating the behaviour and the effect of the Egmond beach- and shoreface nourishment. The major conclusions and recommendations that follow from the evaluation can be found in this chapter.

Starting point for determination of intertidal beach profiles has been the waterline detection model. The first part of this report has been focussed on the applicability and accuracy of this model. Consequently the conclusions that have been drawn from this part of the study are mentioned first, in section 6.2.1. In section 6.2.2. the conclusions about the model results can be found. Finally, section 6.3 describes the recommendations that follow from the conclusions.

6.2 Conclusions

6.2.1 Model

Intertidal beach profiles have been created by modelling waterlines with the waterline detection model. When studying the applicability and the possibility to automate the model, eight cases have been found where meteorological and site specific circumstances cause unacceptable model results. These cases show that color based discrimination of dry and wet pixels can, despite some statistical criteria, not always guarantee sufficiently accurate modelling of the waterline. It is concluded that the waterline detection model can not fully be automated. Sometimes a user defined decision is needed whether or not an Argus image can be used for modelling horizontal waterline coordinates. Still, compared with the timescale of morphologic changes, the high resolution of Argus images in time allows a sufficient amount of model solutions.

During the field campaigns a total of eight successful video recordings of the swashzone have been made in order to determine the location of the waterline in the swash zone. The statistical results from the videos showed that the modelled waterline corresponds with the measured ('glistening') waterline at a location which is crossed by approximately 5% of the runup waves.

The accuracy of the model has been determined by comparing model results with a dataset of DGPS waterline measurements. This allowed an independent validation of on the one hand the Argus based method for finding the horizontal location of the waterline and on the other hand the hydrodynamic modelling of the associated elevation.

In cross-shore direction, the root mean square errors between model and measurements amounted about 5 meters (for 5 to 16 testcases, depending on the longshore location). On a slope 1:40 this can be translated into a rms error in Z of about 13 cm.

In vertical sense the differences between the hydrodynamic model and measurements showed root mean square errors of about 10 cm (27 testcases).

The errors from both submodels can either compensate or amplify the total model error. When taking this effect into account, the root mean square errors for the whole model, expressed as an error in Z , amounted between 5 and 18 cm for locations within 700 m from the Argus cameras.

All of this means the waterline detection model is a quantitative reliable model which is ready for further application. Beside the 'Jan van Speijk' site it will also be applicable at other sites.

6.2.2 Application

Knowing the accuracy and the area of applicability, the waterline detection model has been used to determine time series of intertidal beach profiles of the Egmond beach. It shows the morphologic changes of the intertidal beach between June 1999 and June 2000. Time series of merged images show bar behaviour at the same location. The most important observations that follow from these results are mentioned below:

- From the results it can be found that beach width stays reasonably large near the centre of both nourishments indicating some sort of feeding and/or protective effect of the shoreface nourishment.
- During the stormy season multiple bars shift seaward near this location, bending around the extension of the beach. At the same time the outer bars, including the shoreface nourishment, move landward.
- The former outer bar shows bright wide dissipation patterns behind the centre of the shoreface nourishment whereas to the sides the dissipation patterns weaken. This indicates that the former outer bar varies in height.
- During the summer months of 1999, rip currents can be identified seaward of the erosive zone near $Y = 500$ m. The inner bars move a bit landward at these locations.

On the basis of the observations, two hypothesis are given about the effect and behaviour of both nourishments.

1) The shoreface nourishment disturbs the equilibrium.

This hypothesis considers the shoreface nourishment to be an extra breaker bar. The natural system of four breaker bars (3 bars and 1 swashbar) seems to be disturbed. In search for a new equilibrium the morphological system gets very active. The third and the fourth (former outer bar) breaker bars tend to merge, especially near the centre of both nourishments. This explains why the former outer bar moves landward while normally bars move seaward during stormy winter conditions.

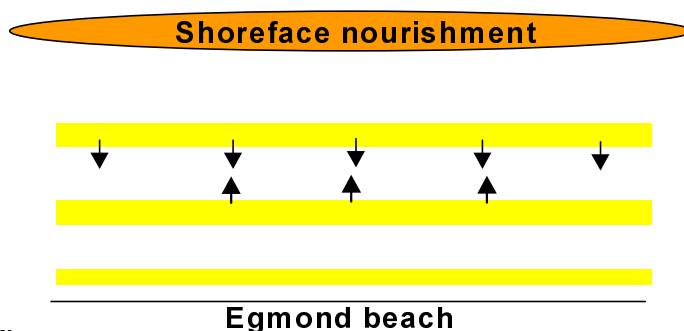


Figure 6.1 Merging bars

2) Former outer bar steers the development on the beach

This hypothesis considers the asymmetric non uniform development of the intertidal beach to be related to the asymmetric former outer bar. Extension of the beach can be found where the presence of the former outer bar is clear. The dissipation patterns show a lot of wave breaking and therefore the beach is to some extent protected against wave attack. To the sides dissipation is less, waves causing more erosion on the beach.

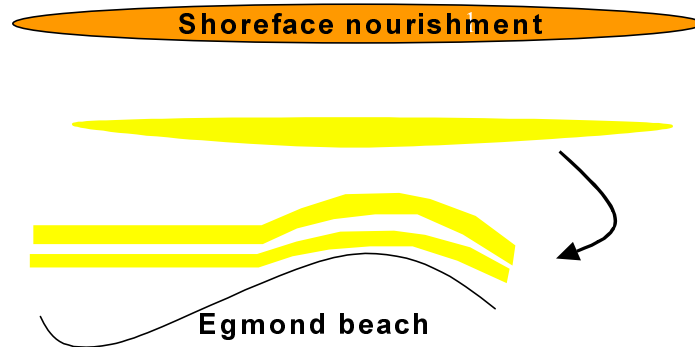


Figure 6.2 Dominant former outer bar

Finally, when considering the expected effects of both nourishments it has been found that beach development is not uniform. The presence of the shoreface nourishment can not prevent this. Still, the intertidal beach shows fast beach recovery. Despite this, the authorities decided to nourish the area between $Y = 0$ and $Y = 1000$ in July 2000.

6.3 Recommendations

6.3.1 Model

The first recommendation concerns the region of interest within an Argus image (see chapter 3, the waterline detection model). Until now the region of interest was fixed and covered most of the image. Any disturbance on the image (rain drop on the lens, sewer pipe in front of camera 4, people on the beach, a car or a boat on the beach, shadows on the beach etc etc..) caused wrong modelling and the image was rejected.

The solution for such a disturbance would be to define the region of interest manually, e.g. with the computer mouse. As a result, smaller or multiple regions of interest are possible within one Argus image. The 'disturbances' can be avoided which increases the amount of solutions. The increase in calculation time will be compensated by the possibility to immediately reject very bad images (rain drops everywhere, darkness, fog, etc..) which are now accepted at first.

Beside local disturbances this might also solve problems concerning longshore color differences (figure 4.11) or areas where the sun shines on the sea.

Because an adjustment like that requires some fundamental changes in the model code this has not been feasible within the time schedule of this study. It might be a good starting point for any future work with the model.

Figure 6.1a shows an example of rain covering the camera lens. Within the region of interest (dotted line) raindrops disturb finding the waterline correctly. In figure 6.1b, the region of interest is user defined to avoid most of the raindrops. In this case the waterline or at least a part of the waterline can still be found.

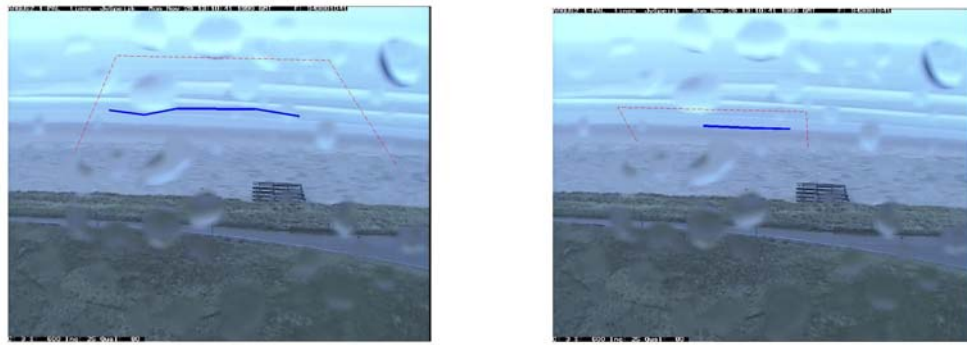


Figure 6.3 Region of interest is chosen automatically (left) and user defined (right)

The last recommendation about the waterline detection technique concerns the combinations of color information that have been used. For the Argus ‘Jan van Speijk’ site it proved that combinations of Hue-Saturation and Hue-Green color information gave the best results. Still, when using the waterline detection model for other Argus sites, other combinations of color information might also show good results. A brief investigation into the possibilities of other combinations of color information might be worth doing (e.g. black and white).

Another possibility might be to change color combinations depending on the time of the day, this can be done manually or automatically.

Nevertheless, it is expected the waterline detection model can easily be applied on the images from other sites.

The next subject for recommendation concerns the method for determining the Z coordinate. First of all the calculation for estimating the tidal level can probably better be replaced by waterlevel measurements in Egmond. Tidal gauges are expected to become operational in July 2000.

Furthermore the calculation of the wave setup with Unibest sometimes becomes unstable when using an equilibrium profile. It might therefore be better to define another bottom profile or to replace Unibest calculations with empirical formulas.

When considering the whole method for finding the vertical waterline coordinate it is recommended to investigate the accuracy of each individual component with additional field measurements. This will make clear which component is causing which error.

6.3.2 Application

Intertidal beach profiles and merged images from the first year of Argus data showed remarkable bar behaviour and non-uniform beach behaviour. It is in this respect recommended to keep monitoring the morphologic changes that occur in front of the lighthouse ‘Jan van Speijk’. The presence of the shoreface nourishment is still visible after a year, the next months or years will make clear which effects are dominant and which are only temporal. Continuation of monitoring will improve the insights about the physical processes that occur. Despite the fact that a new nourishment took place it will still provide an indication of the life span of the shoreface nourishment.

Furthermore it is recommended to study how the morphologic changes of the intertidal beach correspond with the changes on the whole beach. This enables the possibility to define beach developments and morphologic changes of the whole beach in m^3 of sand.

In this respect it would also be useful to investigate relation between the intertidal beach (between NAP 0 m and 1 m) and the BCL-zone (between NAP -5 m and +3 m).

In the conclusions, two hypotheses have been formulated, explaining the possible behaviour and effects of both nourishments. To test the hypotheses it is recommended to quantify beach development with the help of:

- measurements in time: beach profiles, bar heights, currents (direction and velocities)
- numerical models for determining: sediment transport, currents, morphologic changes

With the help of this information in combination with Argus video techniques, the precise effect and behaviour of the Egmond nourishments can be determined.

References

- Aarninkhof, S.G.J. (1996). Quantifications of Bar Bathymetry from Video Observations. Report H2443, DELFT HYDRAULICS.
- Aarninkhof, S.G.J. and Roelvink, J.A. (1999). Argus-based monitoring of intertidal beach morphodynamics. Within the framework of the Marine Science and Technology Programme (MAST III), contractno. MAS3-CT95-0002 and MAS3-CT95-0004.
- Aarninkhof, S.G.J. (1999). Argus & Kustbeheer. Report Z2710, DELFT HYDRAULICS
- Aarninkhof, S.G.J. and van Kessel, T. (1999). Kartering intergetijdestrand uit waterlijnen. Report Z2710, DELFT HYDRAULICS
- Battjes, J.A. (1974). Surf Similarity. Proceedings 14th Int. Conference on Coastal Engineering, ASCE, pp. 466-480.
- Battjes, J.A., and Janssen, J.P.F.M. (1978). Energy Loss and Set-up due to Breaking in Random Waves. Proceedings 16th Int. Conference on Coastal Engineering, ASCE, pp. 569-587.
- Boers, M. (2000). Suppleties bij Egmond en Bergen. Report RIKZ - 99.030. Directoraat-Generaal Rijkswaterstaat, Rijksinstituut voor Kust en Zee.
- Bosboom, J., Aarninkhof, S.G.J., Reniers, A.J.H.M., Roelvink, J.A., Walstra, D.J.R. (1997). Unibest- TC 2.0, overview of model formulations. DELFT HYDRAULICS
- Bruun, P. (1954). Coast Erosion and the Development of Beach Profiles. Beach Erosion Board, Technical Memorandum 44.
- Goda, Y. (1975). Irregular Wave Deformation in the Surf Zone. Coastal Engineering in Japan, Vol 18, pp. 13-26
- Holland, K.T., Holman, R.A., Lippmann, J.S., Plant, N. (1997). Practical Use of Video Imagery in Nearshore Oceanographic Field Studies. IEEE Journal of oceanic engineering, vol. 22, no. 1.
- Holman, R.A., Lippmann, T.C., O'Neill, P.V. and Hathaway, K. (1990). Video estimation of subaerial beach profiles. Marine Geology, 97 (1991), pp 225-231.
- Hunt, I.A. (1959). Design of Seawalls and Breakwaters. Proceedings ASCE, 85, pp. 123-152.
- Janssen, P.C. (1997). Intertidal Beach Level Estimations from Video Images. Report Z2079.20, DELFT HYDRAULICS
- van Koningsveld, M., Mulder, J.P.M., Stive, M.J.F., de Vriend, H.J. (2000). A Methodological Approach towards the embedding of specialist knowledge in ICM processes: From an abstract point of view to a concrete example. Journal of Coastal Research, pp. 701-721.
- Lentz, S. and Raubenheimer, B. (1999). Field observations of wave setup. Journal of geophysical research, vol. 104, no. c11, pages 25,867-25,875.
- Lippmann, T.C., Holman, R.A. (1991). Phase speed and angle of breaking waves measured with video techniques. Coastal Sediments, 1991.
- Lippmann, T.C., Holman, R.A. (1989). Quantification of Sand Bar Morphology: A Video Technique Based on Wave Dissipation. Journal of geophysical research, vol. 94, no. c1, pages 995-1011.
- Munk, W.H., 1949. Surf Beats. Trans. A.G.U., 30, pp. 849-854.
- Plant, N.G. and Holman, R.A. (1997). Intertidal beach profile estimations using video images. Marine Geology 140 (1997) 1-24.
- Roelvink, J.A. (1993). Surfbeat and its effect on cross-shore profiles.
- De Ronde, J.G., van Marle, J.G.A., Roskam, A.P., Andorka Gal, J.H. (1995). Golfstrandvoorwaarden langs de Nederlandse kust op relatief diep water. Report RIKZ - 95.024. Directoraat-Generaal Rijkswaterstaat, Rijksinstituut voor Kust en Zee.
- Shore Protection Manual, (1984). Coastal Engineering Research Center, Department of the Army, Vicksburg, Mississippi.
- Stive, M., Aarninkhof, S., Hamm, L., Capobianco, M., Hanson, H. (1999). (Intra-)seasonal shoreline variability. Within the framework of the Marine Science and Technology Programme (MAST III), contractno. MAS3-CT95-0004.
- Technische Adviescommissie voor de Waterkeringen (TAW), 1995. Basisrapport Zandige Kust, Behorende bij de Leidraad Zandige Kust. (in Dutch).
- van der Velden, E.T.J.M. (1995). Coastal Engineering Volume II. Delft University of Technologie, Department of Civil Engineering.

Wijnberg, K.M.(1995). Morphologic behaviour of a barred coast over a period of decades. Ph.D. Thesis, Utrecht University, Utrecht, The Netherlands, Netherlands Geographical Studies 195, KNAG, 245 pp.

A Existing Argus based methods for finding the waterline

- 1. Intertidal beach profile estimations using video images (Plant and Holman, 1997)**
- 2. Intertidal beach level estimations from video images (Janssen, 1997)**

1. Intertidal beach profile estimations using video images (Plant and Holman, 1997)

To be able to map contours of beach elevation they make use of a visible line that corresponds to the tidal elevation. In the absence of waves this line is the still water level (SWL), which marks contours when moving onshore and offshore during a tidal cycle. In the presence of waves, the SWL is obscured by swash motions and breaking waves. In that case, they use the shoreline intensity maximum (SLIM) on time averaged images as being the visible line.

SLIM behaviour and its relationship with the SWL is a function of different morphodynamic settings. Therefore they quantify SLIM relationships to bathymetry. A general situation at a particular time t_0 and at the horizontal coordinates (x_0 and y_0) of the SLIM is given by:

$$z_{bed}(x_0, y_0, t_0) = z_{tide}(t_0) + \bar{\eta}(x_0, y_0, t_0) - d_{slim}(x_0, y_0, t_0) \quad (1)$$

where z_{tide} is the measured tidal level and η is the total setup at the location of the SLIM. Setup is defined as the elevation of the mean water level above z_{tide} , averaged over a time exposure period. d_{slim} is the mean waterdepth at the SLIM coordinates. The variables are also indicated in figure A.1.

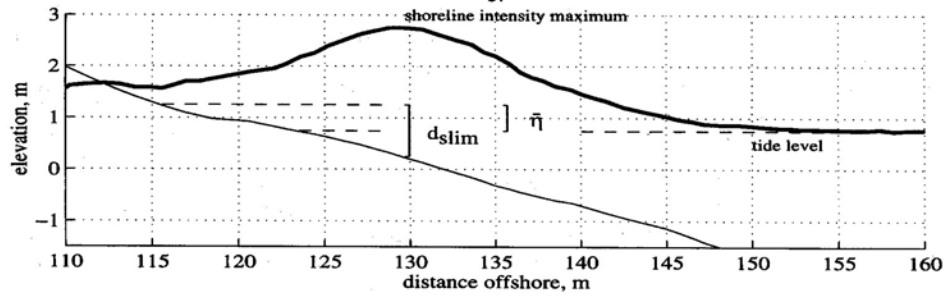


Figure A.1 Definition sketch

The results of their study are based on a field comparison between SLIM bathymetry estimates and accurately surveyed bathymetry. In this way they compare simple processed-based models with empirical models. All of this to be able to test their expectations of the qualitative behaviour of the SLIM's relationship to water depth. Some of the methods used are described below.

To estimate the setup they suggest to use the surf-zone momentum balance equation (Bowen et al. (1968), assuming wave height saturation inside the break point:

$$H = \gamma(h + \bar{\eta}), \quad \text{for } 0 \leq (h + \bar{\eta}) \leq \frac{H_b}{\gamma} \quad (2)$$

where H is the spatially varying wave height, h is the spatially varying still waterdepth, γ is the (constant) ratio of the wave height to water depth and H_b is the wave height at the break point. Assuming a plane sloping beach and integrating from the break point to the shoreline, the total setup at the still water level shoreline is:

$$\bar{\eta}_{swl} \approx \frac{3}{8} \gamma H_b \quad (3)$$

Furthermore Plant and Holman state that on a plain beach, the depth of maximum dissipation increases indefinitely as the incident wave height increases. However on a barred beach, the incident wave height near the shoreline tends to be limited by breaking over the bar. The relevant wave height at the shoreline is that which survives past the bar. Assuming depth saturation of the wave height over the bar they expect that the wave heights at the shore are limited to:

$$H_{shore}(t) = \begin{cases} \mathcal{H}_{bar}(t) & \text{for } H_b(t) \leq \mathcal{H}_{bar}(t) \\ H_b(t) & \text{otherwise} \end{cases} \quad (4)$$

This method is also mentioned here because of this study, where the same approach is used for determining the breaker height responsible for swash (see section 3.3.4).

When assuming low wave height conditions (relative to the water depth over the bar), the bar does not affect the waves climate at the shoreline. They state that the SLIM bathymetry estimation problem can be treated as that of a plane beach. From measurements they expect a simple relationship between the elevation offset and breaking wave height. Setup should be negligible resulting in: $d_{slim} = 0.5H_b$

In conclusion, when trying to find the waterdepth at the SLIM location, the bottom height at this location can be related to d_{slim} (equation 4.1). Measurements showed differences between modelled and measured beach levels in the order of decimeters.

2. Intertidal beach level estimations from video images (Janssen, 1997)

Janssen presents a technique that makes use of black and white video images to find horizontal coordinates of the waterline. The vertical waterline coordinate is found by cross-shore hydrodynamic modelling. The combination of both gives the location of the waterline. By taking all images during one tidal cycle into account he finds multiple waterlines, hence the intertidal beach bathymetrie.

Beside time averaged images, Janssen makes use of standard deviation images or in other words variance images. These images provide the standard deviation of the average intensity in time of each pixel. Hence they indicate regions of fluctuating image intensity, typically what happens in the area where waves break.. Janssen identifies the waterline from a cross-shore correlation analysis between the cross-shore image intensity profile and the variance profile, which yields a location in the higher part of the swash zone.

A small dataset of field measurements showed root mean square differences between calculated and measured waterlines to be intra swash (typically 5 to 8 m). On the other hand he often finds a phase shift and sometimes a weak correlation between the intensity signal from time averaged images and the standard deviation signal from variance images. This caused difficulties trying to find the waterline.

Hydrodynamic modelling of the waterline z-coordinate was split up in accordance with the phenomena which contribute to the total runup level, he defined: Wave setup, wind setup, swash of individual waves and surfbeat.

The wave setup was modelled with the cross shore wave decay module of UNIBEST-TC. For the underlying bottomprofile an equilibrium profile according to Bruun (1954) was

used. The only parameter that was calibrated in respect of the wave setup is the wave height, indicating errors of about 5 %.

The total runup level showed more sensitivity for an error in beach slope or bar height. Variation within realistic boundaries showed z-coordinate variations order 0-10 cm.

In conclusion, the waterline detection technique based on variance images showed some good results. In spite of that the technique has not been developed any further, mainly because it turned out to be a complicated method which was hard to make operational. Part of the method of finding the waterline z-coordinate has been adopted into this study and is treated in section 3.3.

B Cases at where the waterline detection model is not appreciable

C Calculations for the vertical waterline coordinate

- 1. The Unibest wave module**
- 2. Calculation of the wave runup/rundown**

1. The Unibest wave module

The wave propagation model consists of three first-order differential equations, viz. the time averaged wave energy balance (Battjes and Janssen, 1978), the balance equation for the energy contained in surface rollers in breaking waves (Nairn et al., 1990) and the horizontal momentum balance from which the mean water level set-up is computed. The refraction of the waves is computed using Snel's law. The three coupled equations can be solved by numerical integration over the cross-shore profile.

The energy balance equation for organised wave energy E reads

$$\frac{\partial}{\partial x}(EC_g \cos \theta) = -D_w - D_f \quad (1)$$

Where C_g is the wave group velocity, θ the angle of incidence of the wave field, D_w the dissipation of wave energy due to breaking and D_f the dissipation due to bottom friction. The organised wave energy E is defined according to linear wave theory

$$E = \frac{1}{8} \rho g H_{rms}^2 \quad (2)$$

where ρ is the density of water, g the gravitational acceleration and H_{rms} the root mean square wave height.

Battjes and Janssen use as a closure for this an expression for the dissipation of organised wave energy based on a bore model.:

$$D_w = \frac{1}{4} \rho g \alpha f_p H_{max}^2 Q_b \quad (3)$$

where $f_p = 1/T_p$ is the peak frequency, Q_b the fraction of breaking waves and α a dissipation coefficient, which equals 1 in case of a fully developed bore. The model applies a so-called clipped Rayleigh through the surf zone, assuming that the waves smaller than H_{max} are not breaking and Rayleigh distributed, and that all waves larger than H_{max} are breaking. This maximum wave height H_{max} is defined as a function of the local water depth, according to:

$$H_{max} = \frac{0.88}{k} \tanh\left(\frac{\gamma k h_r}{0.88}\right) \quad (4)$$

where k is the local wave number, h_r the local waterdepth (which was modified later on by Roelvink et al. (1995), and γ a dissipation coefficient. Battjes and Stive (1985) performed an extensive calibration study for γ , based on both field and laboratory data.

Setting α equal to 1, the best fit values for γ turned out to vary systematically with the offshore wave steepness $s_0 = H_{rms,0}/L_0$, according to

$$\gamma = 0.5 + 0.4 \tanh(33s_0) \quad (5)$$

Equation 5 expresses the default relationship for γ as applied by UNIBEST-TC. The fraction of breaking waves Q_b reflects the percentage of waves larger than H_{\max} and is computed iteratively from

$$\begin{aligned} \frac{1-Q_b}{\ln(Q_b)} &= -\left(\frac{H_{rms}}{H_{\max}}\right)^2 & \text{for } \frac{H_{rms}}{H_{\max}} < 1 \\ Q_b &= \left(\frac{H_{rms}}{H_{\max}}\right)^2 & \text{for } \frac{H_{rms}}{H_{\max}} \geq 1 \end{aligned} \quad (6)$$

Though ‘impossible’ from a theoretical point of view, it may occur that the value of H_{rms} exceeds the value of H_{\max} in very shallow water (frequently in combination with plunging breakers). In those situations the second formulation of Eq.6 is applied, which in fact implies that the maximum wave height H_{\max} in Eq.3 is replaced by the local wave height H_{rms} , hence introducing extra wave dissipation in a region where H_{rms} actually is too large. Finally the wave dissipation D_f due to bottom friction, which is the second sink term in Eq. 3.1, is modelled as

$$D_f = \frac{f_w \rho}{\sqrt{\pi}} u_{orb}^3 \quad (7)$$

where f_w is a user defined friction factor (FWEE) and u_{orb} the amplitude of the wave orbital velocity based on linear wave theory and the rms wave height.

Investigation of model performance learned that model predictions of wave height decay were reasonably well in correspondance with wave height measurements through the surf zone, however, the location of initial set-up was predicted too far seaward. For that reason the roller model according to Nairn et al. (1990) has been incorporated in UNIBEST-TC. Instead of being dissipated immediately after the breakpoint, organized wave energy is converted into turbulent kinetic energy first (which can be seen from the development of a roller at the face of a breaking wave), before being dissipated ultimately via the production of turbulence. In this way the dissipation process is delayed, hence shifting the region of wave set-up in shoreward direction. This roller model provides the second differential equation of the UNIBEST model, the roller balance equation:

$$\frac{\partial}{\partial x}(2E_r C \cos \theta) = D_w - Diss \quad (8)$$

In this expression, c is the wave propagation speed, $Diss$ the dissipation of roller energy and D_w the dissipation of organised wave energy which acts as a source term for the roller balance equation. The factor ‘2’ in Eq. 3.8 originates from additional dissipation of roller energy due to a net transfer of water from the wave to the roller (Stive and De Vreind, 1994). The roller energy represents the amount of kinetic energy in a roller with area A and length L , and is defined as

$$E_r = \frac{1}{2} \rho c^2 \frac{A}{L} \quad (9)$$

The roller energy balance is closed by modelling the dissipation $Diss$ of roller energy as the power per unit length performed by the shear stress between roller and water surface:

$$Diss = \beta \rho g c \frac{A}{L} = 2\beta g \frac{E_r}{C} \quad (10)$$

where β is the slope of the face of the wave (normally in the range 0.05-0.10) and A is written in terms of E_r via Eq. 3.9.

In order to improve the prediction of bar morphodynamics, Roelvink et al. (1995) introduced their concept of breaker delay. The dissipation of organised wave energy as computed from Eq.3 and 4 is only based on local waterdepth, and disregards the fact that waves need a distance in the order of one wave length to actually start or stop breaking. For that reason they suggest to take into account the bottom elevation some distance seaward of the computational point when determining the water depth h_r to be applied in Eq.4. To that end they define a reference depth h_r , obtained from weighting water depths seaward of the computational point via a weighing function $W(\xi)$:

$$h_r(x) = \frac{\int_{x-X}^x W(x-x') h(x') dx'}{\int_{x-X}^x W(x-x') dx'} \quad (11)$$

In this expression, h is the local waterdepth and X is the integration distance. The weighting function W is given by:

$$W(\xi) = (X - \xi)^p \quad (12)$$

where p is a user defined parameter which determines the shape of the weighting function. The integration distance X is taken proportional to the local peak wave length L_p :

$$X = \lambda L_p \quad (13)$$

where λ is a user defined coefficient of order one.

The third differential equation is the cross-shore momentum equation or set-up equation, which reads:

$$\frac{\partial \bar{\eta}}{\partial x} = -\frac{1}{\rho g h} \frac{\partial S_{xx}}{\partial x} \quad (14)$$

Here, η is the mean wave set-up, $h = \bar{\eta} - z_b$ the local water depth and S_{xx} the cross shore radiation stress, which is defined as

$$S_{xx} = \left((n + n \cos^2 \theta - 0.5) E + 2 E_r \cos^2 \theta \right) \quad (15)$$

where $n = C_g/C$, the ratio between wave propagation speed and the group velocity. The wave direction θ is defined as the angle between the x-axis (perpendicular to the shoreline, positive landwards) and the propagation direction is found from Snel's law:

$$\frac{\sin \theta}{\sin \theta_0} = \frac{C}{C_0} \quad (16)$$

where the subscript 0 refers to values at the seaward boundary of the model.

Finally the propagation speed C is defined as

$$C = \frac{\omega}{k} \quad (17)$$

where $\omega = 2\pi f_p$ is the angular frequency, and k is the wave number, which is solved from the dispersion relation:

$$\omega^2 = gk \tanh(kh) \quad (18)$$

In order to solve the system for the three unknown E , E_r and η , boundary conditions for E , E_r , η and θ and a bottom profile $z_b(x)$ are needed; The boundary value of E is computed from Eq. 2. via a user defined wave height at the upwave boundary. In addition, θ and $z_b(x)$ should be given at the upwave boundary, while η is set to zero which is reasonable if the upwave boundary is located outside the surfzone. The roller energy E_r at the seaward boundary is estimated from Eq. 10, assuming that D_{ss} equals D_w . Coefficient values must be given for α (default value 1), γ (default value given by Eq. 5), β (optimum value between 0.05 and 0.10) and λ (value of order 1).

In this study, the parameter set default values are used, meaning:

$$\alpha = 1.00;$$

$$\gamma = 0.65;$$

$$\beta = 0.20;$$

$$\lambda = 1.00;$$

$$f_w = 0.01; \text{ (the wave friction factor)}$$

2. Calculation of the runup/rundown

The calculation starts with an estimation of the inner bar height, in this study at NAP -0.5 m. The difference between the tidal level and the inner bar height determines the ‘limited’ depth. The waves able to pass this limited depth will break in front of the beach, they are responsible for swash. Thus:

$$h_{Lim} = z_{Tide} - h_{bar} \quad (19)$$

Consequently, at low tides when the inner bar is exposed ($h_{Lim} \leq 0$), the runup height is zero. For all cases where $h_{Lim} > 0$, the computation starts with a calculation of the breakerdepth using linear wave theory.

The required parameters from the wave database are: the significant wave period (T_{sig}), the angle of incidence (φ_0) and the significant wave height (H_{sig}). The deep water wave length respectively the deep water wave speed are computed by:

$$L_0 = \frac{gT_{sig}^2}{2\pi} \quad \text{and} \quad c_0 = L_0 / T \quad (20)$$

Because depth contours are assumed to be parallel, an iterative scheme is used:

First step is a guess of the breakerdepth h_b . The wave length at the breaking point reads:

$$L = \frac{gT_{sig}^2}{2\pi} \cdot \tanh\left(\frac{2\pi h_b}{L}\right) \quad (21)$$

Iteration is necessary to find L. Next is a calculation of the shoaling parameter:

$$K_{sh} = \sqrt{\frac{1}{\left(1 + \frac{2kh_b}{\sinh(2kh_b)}\right) \tanh(kh_b)}} \quad \text{and} \quad k = 2\pi/L \quad (22)$$

Refraction changes the angle of incidence, at the breaking point the angle is:

$$\sin(\varphi_b) = (c / c_0) \sin(\varphi_0) \quad (23)$$

$$c = \frac{gT_{sig}}{2\pi} \tanh(kh_b) \quad (24)$$

Finally the (significant) breakerheight reads:

$$H_b = H_{sig} \cdot K_{sh} \cdot \sqrt{\frac{\cos(\varphi_0)}{\cos(\varphi_b)}} \quad (25)$$

A new value for h_b is computed from the known values of γ and the computed H_b ($h_b = H_b/\gamma$). The iterative computation returns to equation 4.19 until the correct h_b is found.

Before computing the runup height, the model checks if the breaking depth (h_b) is not limited by the limited depth above the inner breaker bar. Thus, if $h_b < h_{Lim}$, it is the wave height H_b which causes swash. If the depth is limited, $h_b > h_{Lim}$, a new H_b needs to be calculated by: $H_b = \gamma \cdot h_{Lim}$.

A well accepted empirical formula for the runup height of waves breaking on a smooth slope is a formula by Hunt (1959), written as:

$$\frac{R_u}{H} = \xi \quad \text{for } 0.1 < \xi < 2.3 \quad (26)$$

the Iribarren or similarity parameter reads:

$$\xi = \frac{\tan \alpha}{(H / L_0)^{1/2}} \quad , \tan \alpha \text{ is the bottom slope} \quad (27)$$

Assuming the local wave height H causing runup to be equal to the breaking wave height results in:

$$\xi_b = \frac{\tan \alpha_b}{(H_b / L_0)^{1/2}} \quad (28)$$

Battjes and Roos (1974) did measurements of the runup of breaking waves on dike slopes. When analysing their measurements, they found an expression for the rundown height R_d , defined as the minimum elevation of the waterline above the undisturbed water level. The expression reads:

$$R_d = (1 - 0.4\xi)R_u \quad (29)$$

valid for the experimental range: $\cot \alpha = 3, 5, 7, 10$; $0.02 < H/L_0 < 0.09$ and $0.3 < \xi < 1.9$.

H is the wave height at the toe of the slope and R_u the runup height.

From this formula they conclude that the ratio of the variable part of the vertical motion of the waterline ($R_u - R_d$) to the maximal elevation above still water level is approximately 0.4ξ . They state that it has a maximal value of about 1 for waves in the transition zone between breaking and non-breaking.

The difference between runup and rundown, hence the height of the swash zone is:

$$S_v = R_u - R_d \quad (30)$$

Both terms are defined relative to the undisturbed waterlevel. When assuming that R_d is always below still waterlevel the formula reads:

$$S_v = R_u + R_d \quad (31)$$

Substitution of 4.24 and 4.27 gives:

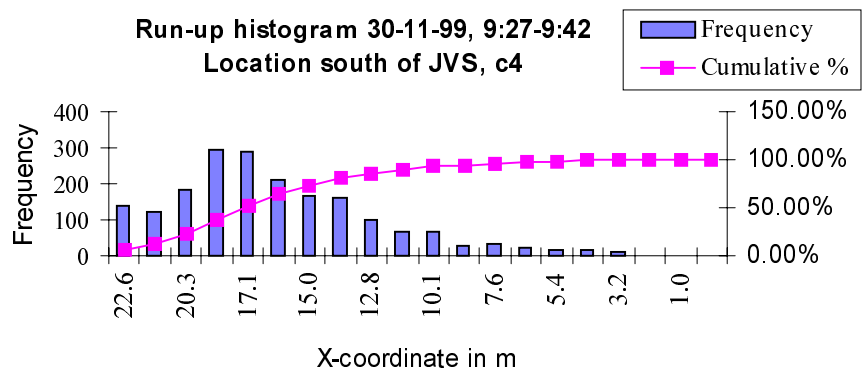
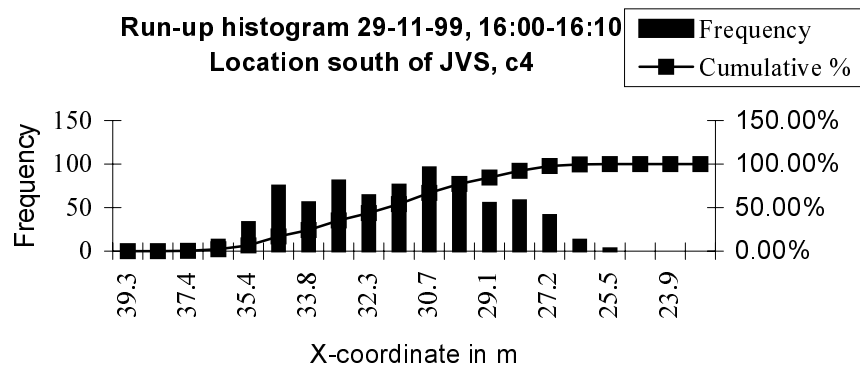
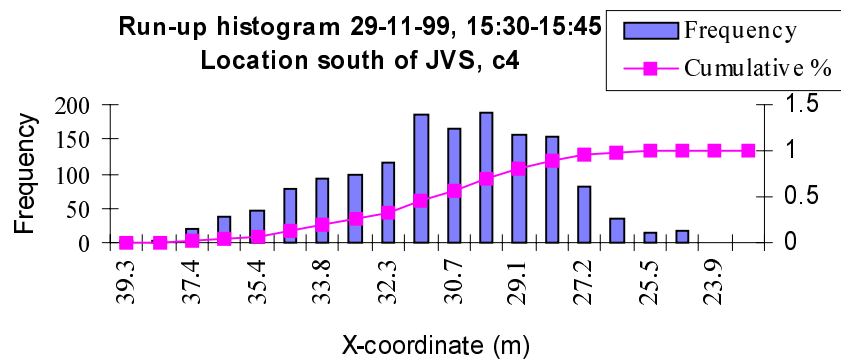
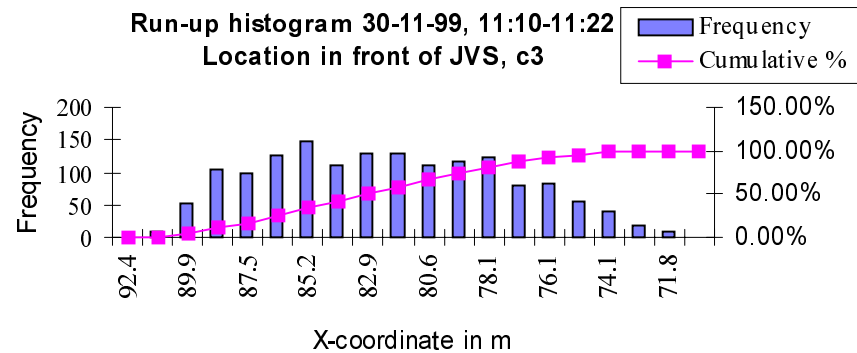
$$S_v = (2\xi_b - 0.4\xi_b^2)H_b \quad (32)$$

It is this formula that has been applied in the waterline detection model for calculation of the swash height.

D Results from the swash videos

- 1. Swash video statistics from the November campaign**
- 2. Measured and (if available) modelled horizontal waterline in the swash zone + the swash zone locations of 5% respectively 95 % exceedence.**

1. Swash video statistics from the November campaign



2. Measured and (if available) modelled horizontal waterline in the swash zone + the swash zone locations of 5% respectively 95 % exceedence.

E Waterline measurements

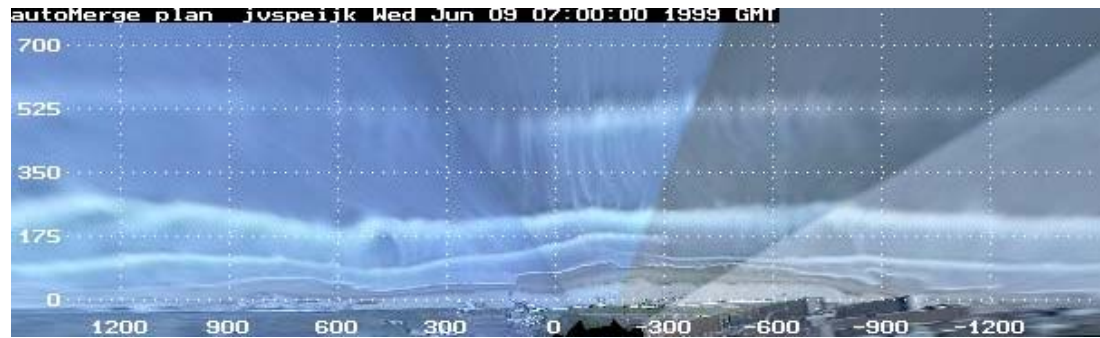
- **Example of waterline measurements in X-Y for 29-11-1999**
- **Example of waterline measurements in Y-Z for 29-11-1999**

F Egmond morphology

- **Measured and modelled profiles of November and March**
- **Intertidal beach development between June 1999 and June 2000**
- **Bar behaviour between June 1999 and June 2000**
- **Stacked images along transects $Y = -250$ m and $Y = 600$ m**

- Bar behaviour between June 1999 and June 2000

June 1999



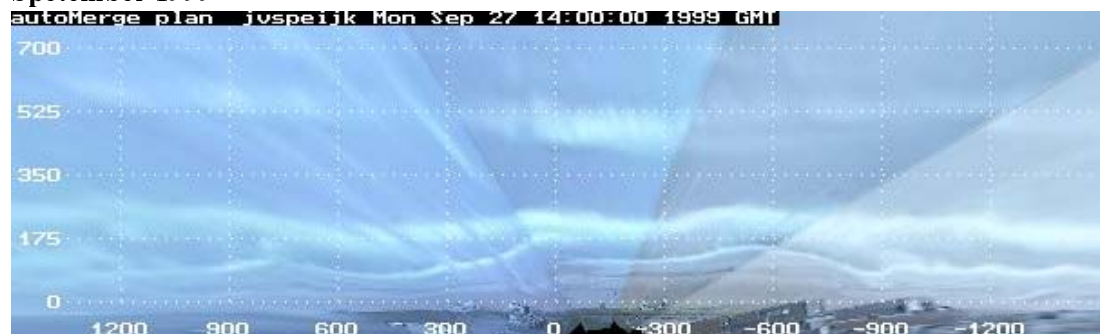
July 1999

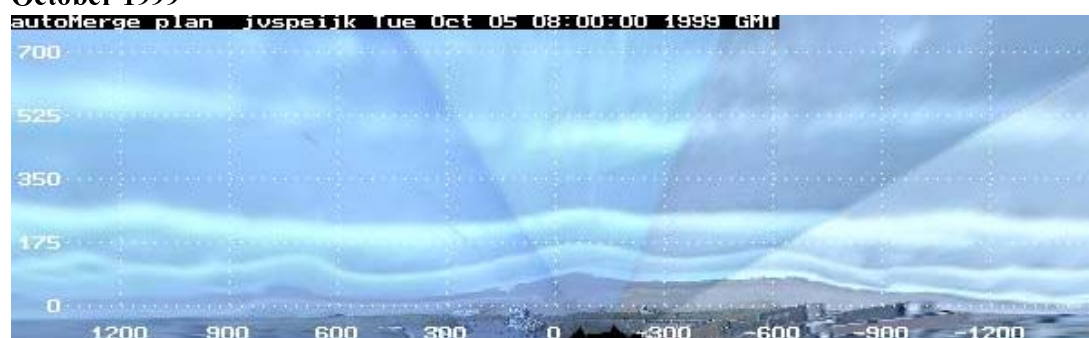
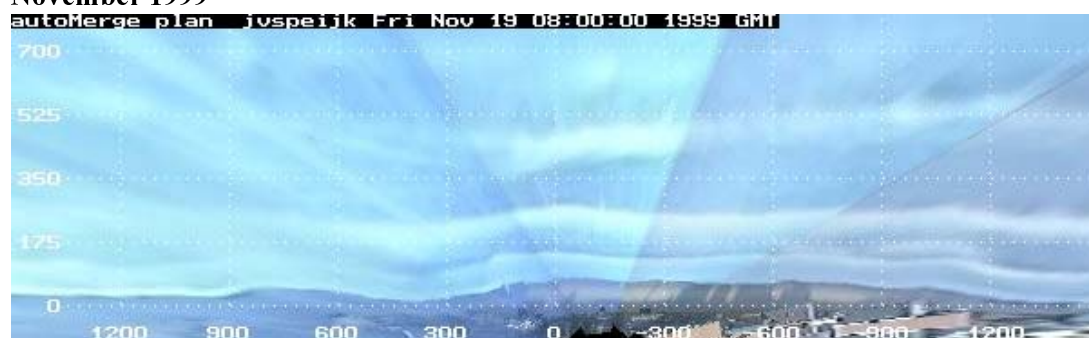


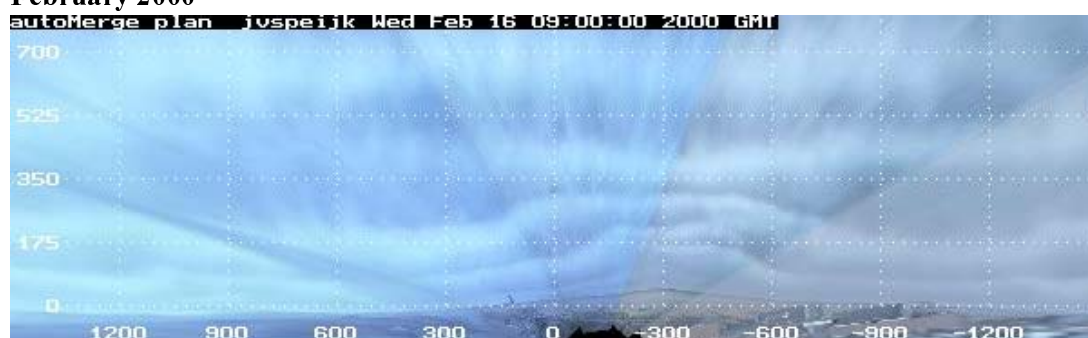
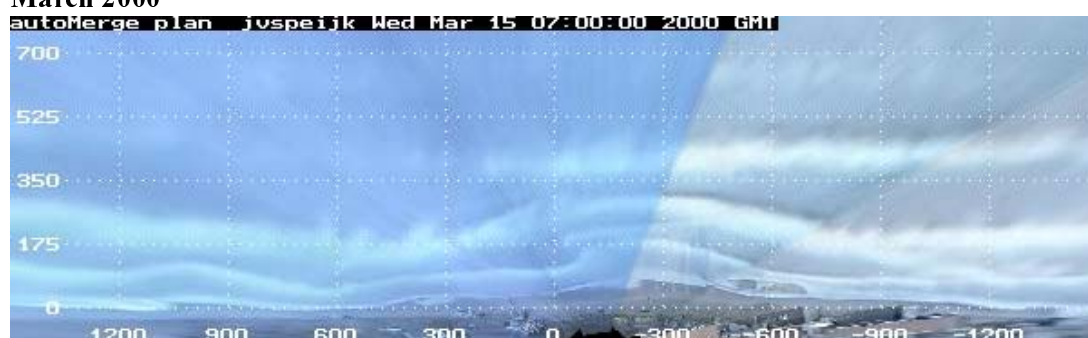
August 1999



Spetember 1999



October 1999**November 1999****December 1999****January 2000**

February 2000**March 2000****April 2000****May 2000**

June 2000